IOP Publishing Journal of Physics B: Atomic, Molecular and Optical Physics

J. Phys. B: At. Mol. Opt. Phys. **57** (2024) 212001 (18pp) https://doi.org/10.1088/1361-6455/ad7cac

Topical Review

Advances in timing and control of ultrafast molecular dynamics: from XUV to infrared

Wenyu Jiang[1], Shengzhe Pan[1], Hao Huang[1], Jihong Tong[1], Wenbin Zhang[1], Hongcheng Ni[1,2,*] and Jian Wu[1,2,3]

[1] State Key Laboratory of Precision Spectroscopy, East China Normal University, Shanghai 200241, People's Republic of China
[2] Collaborative Innovation Center of Extreme Optics, Shanxi University, Taiyuan, Shanxi 030006, People's Republic of China
[3] Chongqing Key Laboratory of Precision Optics, Chongqing Institute of East China Normal University, Chongqing 401121, People's Republic of China

E-mail: hcni@lps.ecnu.edu.cn

Received 18 December 2023, revised 27 August 2024
Accepted for publication 18 September 2024
Published 9 October 2024

Abstract

With the availability of modern laser and detection technologies, the investigation of ultrafast molecular dynamics induced by intense laser pulses has become a routine practice. In this Topical Review, we present a survey of recent progress in the timing and control of ultrafast molecular dynamics, encompassing processes initiated by both extreme ultraviolet and near infrared pulses. Prospects and perspectives of this field are given. This Review underscores the remarkable potential for further advances in understanding and harnessing ultrafast molecular processes.

Keywords: molecular dynamics, chemical reaction, attosecond time resolution, photoionization delay, ultrafast stopwatch

1. Introduction

As laser and detection technologies continue to advance, the exploration of ultrafast dynamics of molecules interacting with intense laser pulses has evolved into a standard practice. In the 1980s, the maturation of femtosecond lasers enabled the temporal resolution of chemical reactions occurring on the femtosecond timescale, marking the birth of femtochemistry [1]. About 20 years later, this breakthrough was recognized with Zewail's Nobel Prize in Chemistry 1999, awarded 'for his studies of the transition states of chemical reactions using femtosecond spectroscopy'. In femtochemistry, the time resolution is achieved typically through the femtosecond pump–probe setup, where a femtosecond pump pulse initiates the ultrafast molecular dynamics, and a time-delayed femtosecond probe pulse monitors the dynamical evolution of the molecule. The advent of high-order harmonic generation (HHG) [2–9] allowed for the table-top production of attosecond laser pulses [10, 11] in the 2000s. This development enabled the temporal resolution of electronic processes within atoms [12], molecules [13], liquids [14, 15], solids [16, 17], and at the nanoscale [18], heralding the era of attosecond physics [19, 20]. About another 20 years later, Agostini, Krausz, and L'Huillier were award the Nobel Prize in Physics 2023 'for experimental methods that generate attosecond pulses of light for the study of electron dynamics in matter'. Despite the thriving attosecond physics, achieving attosecond time resolution via attosecond pump and attosecond probe is still a major challenge, due to the difficulty

* Author to whom any correspondence should be addressed.

© 2024 IOP Publishing Ltd. All rights, including for text and data mining, AI training, and similar technologies, are reserved.

to balance the pulse energy and the repetition rate as well as the inherently low cross section of attosecond pulses, typically in the extreme ultraviolet (XUV) regime, when interacting with matter [21–23]. Therefore, a near infrared (NIR) femtosecond pulse is still used, by exploiting its known subcycle modulation, to achieve attosecond temporal resolution. Frequently used techniques include the attosecond streak camera [11, 24], the reconstruction of attosecond beating by interference of two-photon transitions (RABBITT) [10, 25], and the attoclock [26–28].

Except the shortening of the laser pulse and the corresponding increasing temporal resolution, the coincidence detection technology has been indispensable for the investigation of ultrafast molecular dynamics. The reaction microscopy of the cold target recoil ion momentum spectroscopy (COLTRIMS) [29] allows for the measurement of the full three-dimensional momentum vector of both the electron and the recoiling target ion resulting from ionization events with high resolution. The measurement with full solid angle is enabled by the magnetic field added in the reaction region that guides all charged particles to the detector. The three-dimensional momentum vector of the charged particles can be reconstructed by analyzing their time-of-flight (TOF) and position-of-impact on the detector. Furthermore, the COLTRIMS setup has the capability to detect multiple particles in coincidence, enabling the differentiation of correlated particles based on momentum conservation. This feature allows for the isolation of individual ionization events and reaction channels. It, therefore, offers a robust platform for investigating the underlying physical mechanisms of various correlated phenomena, such as the dynamics of molecular bond cleavage, electron–nuclear correlations during molecular dissociation, and more.

This Topical Review presents an overview of recent advancements in the temporal control and manipulation of ultrafast molecular processes. The scope encompasses processes initiated by both XUV and NIR pulses. In the following, we start from the ultrafast molecular dynamics initiated by XUV pulses, to those launched and modulated by NIR pulses, covering an extended spectral range of the driving laser. As the wavelength of the driving laser increases, the ionization process transitions from multiphoton to tunneling ionization. In multiphoton ionization, the target perceives the light as discrete photon energies, and the laser is characterized in the frequency domain. This leads to the familiar realm of photochemistry. Conversely, in tunneling ionization, the target interprets the light pulse as a classical electromagnetic field, with the laser being represented in the time domain. By precisely shaping the temporal structure of the laser pulse, it becomes possible to steer the reaction dynamics of molecules in a controlled fashion in the time domain. This advancement ushers in the promising field of 'optochemistry' [30, 31], which introduces innovative methods for manipulating light-induced ultrafast molecular chemical reactions in the time domain, extending beyond the boundaries of conventional photochemistry. As we delve into the developments in ultrafast molecular dynamics, we also outline the prospects and perspectives that lie ahead in this dynamic field. By highlighting the progress made, we aim to underscore the considerable potential for further breakthroughs in understanding and harnessing ultrafast molecular processes.

2. Photoionization delay in perturbative regime

Photoionization time delay plays a pivotal role in the study of light–matter interactions, acting as an exquisite probe that reveals subtle differences in potential energy surfaces (PES). These differences are often linked to the intrinsic properties of elements [32], complex resonances [33–36], and the dynamic stretching and compression of molecular bonds during the photoionization process. In comparison to a freely propagating wave packet, a wave packet interacting with a potential experiences an additional phase shift. This shift contains valuable information about the potential, which is at the heart of the well-known Eisenbud–Wigner–Smith (EWS) photoionization time delay [37, 38]. Advanced attosecond interrogation techniques [20] have been instrumental in further exploring these time delays. These include the attosecond streak camera [11, 24], the RABBITT technique [10, 25], and the attoclock [26–28]. These techniques have found broad application in investigating time delays in atoms, molecules, and condensed phase matter, expanding our understanding of ultrafast processes in these systems.

Among these techniques, the RABBITT technique employs an XUV attosecond pulse train (XUV-APT) from HHG and a weak NIR probe field to establish an attosecond interferometry. As depicted in figure 1, the typical signature of this technique is the formation of sideband (SB) photoelectrons in the spectrum, situated between two consecutive main-peak photoelectrons that are directly ionized by the XUV-APT. Within the framework of lowest-order perturbation, these SB photoelectrons originate from the interference between two pathways: (1) absorption of one HHG photon at the frequency of $(2q-1)\,\omega_{\mathrm{NIR}}$ and one NIR photon at ω_{NIR}, and (2) absorption of one HHG photon at the frequency of $(2q+1)\,\omega_{\mathrm{NIR}}$ and emission of one NIR photon at ω_{NIR}. As a result, the SB yield oscillates with the pump–probe time delay τ as:

$$P_{\mathrm{SB}} = A\cos\left(2\omega_{\mathrm{NIR}}\tau - \phi_0^{2h\nu}\right) + B,$$

where $\phi_0^{2h\nu}$ is the oscillation phase given by $\phi_0^{2h\nu} = \Delta\phi_{\mathrm{XUV}} + \Delta\phi_{\mathrm{EWS}} + \Delta\phi_{\mathrm{CC}}$, and A and B are fitting parameters. Here, $\Delta\phi_{\mathrm{XUV}}$ and $\Delta\phi_{\mathrm{EWS}}$ represent the difference in the harmonic phase and the one-photon scattering phase between consecutive harmonics, respectively, and $\Delta\phi_{\mathrm{CC}}$ is the continuum—continuum (CC) transition phase shift associated with the emission and absorption of one NIR photon [39, 40]. Thereby, the associated term of time delay τ_{EWS} is referred to the one-photon ionization time delay [37, 38] and τ_{CC} as the CC time delay [40], respectively. In experimental practice, the influence of $\Delta\phi_{\mathrm{XUV}}$ can be eliminated by comparing SBs of the same order from different targets through simultaneous measurements.

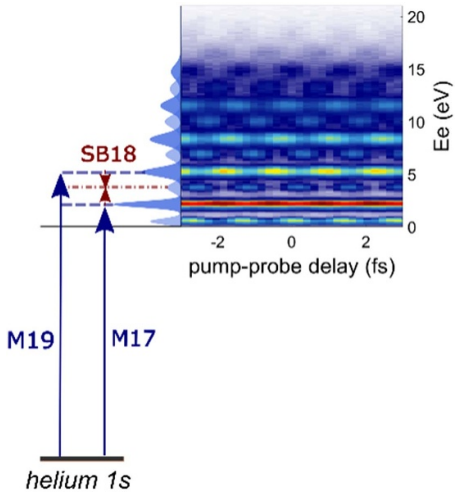

Figure 1. The principle of SB generation in helium with a XUV-APT covering harmonics from the 15th to the 25th order. Reproduced from [41], with permission from Springer Nature.

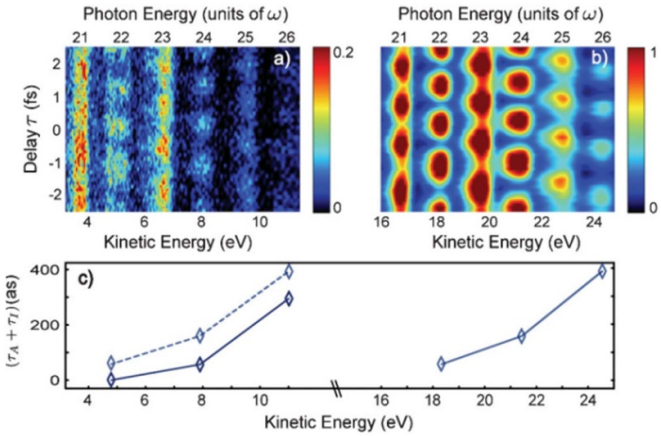

Figure 2. RABBITT spectrum of photoelectrons from the (a) 3*s* and (b) 3*p* shell of argon. (c) The corresponding reconstructed time delays. Reprinted figure with permission from [32], Copyright (2011) by the American Physical Society.

2.1. Energy-resolved photoionization time delay in atoms and molecules

To investigate photoionization time delays, various detection techniques have been applied to collect the spectroscopic data of electrons and ions. By integrating a magnetic bottle electron spectrometer, which records the TOF of electrons [42], Klünder *et al* revealed different time delays between photoelectrons emitted from the $3s^2$ and $3p^6$ shells in argon, as shown in figure 2. Shortly after, the relative delay among different noble atoms [43] were reported, which indicates that the photoionization time delay can sensitively probe the Coulomb and centrifugal potentials.

Although the TOF spectroscopy lacks the spatial resolution, its high spectral resolution enable to alleviate the spectral congestion in molecules where the signals from different molecular orbitals overlap in the photoelectron energy spectrum. Huppert *et al* reported the relative two-photon ionization time

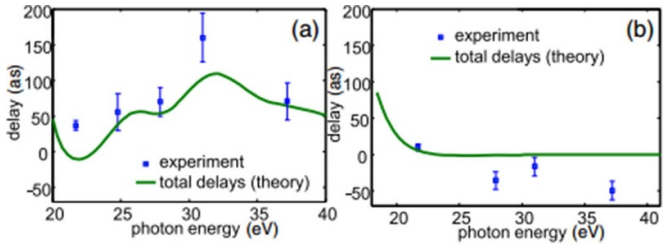

Figure 3. Relative time delay between $\widetilde{A}^+$and $\widetilde{X}^+$states in (a) N_2O^+ and (b) H_2O^+. Reprinted figure with permission from [33], Copyright (2016) by the American Physical Society.

delays between the $\widetilde{A}^+$and $\widetilde{X}^+$states in N_2O and H_2O using the magnetic bottle electron spectrometer, within a photon energy range of 20 eV to 40 eV [33], with results shown in figure 3. A significant delay originating from the molecular shape resonance up to 110 as was revealed, which was notably absent in H_2O, marking the first real-time observation of this well-known molecular shape resonance. A later work, with a high energy resolution, distinguished the vibrational levels of X and A states in non-dissociative ionization of N_2 [34]. The time delay difference between X and A electronic states for $\nu' = 0$ displayed an enhancement corresponding to the $3\sigma_g^{-1}$ shape resonance in the X state. The difference between $\nu' = 1$ and 0 vibrational levels provided clear evidence of non-Franck–Condon ionization dynamics, indicating that the nuclear motion influences the emitted photoelectrons. The nuclear–electron coupling effect was further verified in vibrational-state-resolved photoionization time delays in H_2 using the same TOF spectroscopy [44].

Further studies have observed photoionization time delays resulting from spin–orbit splitting [45], Cooper minima [46] and the Fano autoionization resonance [35, 36], all of which require a high energy resolution to distinguish, using the same detection method. Additionally, by varying the wavelength of the fundamental laser field to produce high harmonics, the resonant two-photon phase shifts through Rydberg states as the function of the detuning was revealed in helium [47].

Recently, the application of detection techniques with multi-dimensional momentum resolution, such as the velocity map imaging (VMI) [48] and COLTRIMS [29], has enabled the detection of attosecond nondipole effects along the laser propagation direction [49]. Attosecond interferometry has been further applied to study two- and three-dimensional hydrocarbons, which shows that the photoionization time delay between these 2D and 3D molecules is associated with quadrupole effects. It also indicates that in complex molecules, the photoelectron time delays are influenced by both the symmetry and the shape of the initial orbital from which the photoelectron emits [50]. Different from the VMI technique, the multi-particle COLTRIMS setup allows for the differentiation of photoelectrons from various ionization channels through coincident measurements with ionic fragments, and thus can be used to measure photoionization time delays arising from two-center interference in the Kr_2 [51], ion–electron correlation effects in H_2 [52], electron correlation effects in shake-up processes [53] and between dissociative and non-dissociative

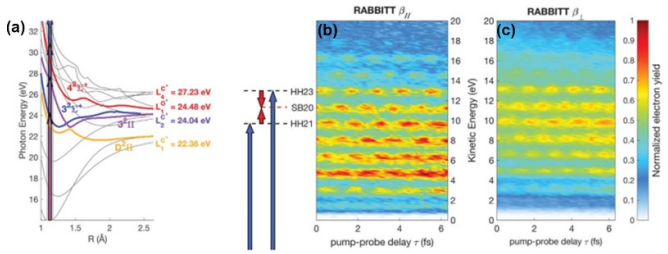

Figure 4. (a) Potential energy curve of the CO^+ molecular ion. (b) The RABBITT spectrum for molecules oriented along the laser polarization axis. (c) The RABBITT spectrum for molecules oriented perpendicular to the laser polarization axis. From [55]. Reprinted with permission from AAAS.

ionization channels in CH_4 and CD_4 [54]. Also, this 3D momentum spectroscopy has enabled the detection of attosecond nondipole effects along the laser propagation direction [49].

2.2. *Photoionization delay in the molecular frame*

In the study of molecules, coincidence measurements have been employed to reveal orientation-dependent, emission-angle-resolved time delays in the molecular frame, based on the recoil axis approximation. The stereo Wigner time delay for CO, defined as $\tau_{\mathrm{S-EWS}} = \tau_{\mathrm{EWS}}^{(\text{carbon side})} - \tau_{\mathrm{EWS}}^{(\text{oxygen side})}$, was first reported by Vos *et al* in 2018 [55]. Based on the axial recoil approximation, which assumes that molecular dissociation occurs much faster than its rotation, the relative angle, β, between the molecular axis and the laser polarization axis at the momentum of ionization can be determined. By averaging over an opening angle of $\pm 20°$, the photoelectrons produced from the parallel and perpendicularly orientated CO can be selectively analyzed, as shown in figures 4(b) and (c). Consequently, the $\tau_{\mathrm{S-EWS}}$ as a function of electron energy for both parallel and perpendicular orientations was revealed. For the parallel case ($\beta_{\parallel}$), $\tau_{\mathrm{S-EWS}}$ exhibited a negative value, gradually approaching zero with increasing electron energy. By combining theoretical simulations of the ionization dynamics initiated by the XUV pulse and a classical Wigner propagation method for the two-photon process, the observed $\tau_{\mathrm{S-EWS}}$ was attributed to the asymmetric initial electron populations in the specific ionic states, reflecting the relative mean position of the photoelectrons at the moment of ionization.

Subsequently, Heck *et al* [56] reported on the shape-resonance-induced photoionization time delay for two-photon ionization from the HOMO and HOMO-1 orbitals in CF_4 with respect to argon. At the same time, the angle-resolved photoionization delays in the recoil frame were investigated, as shown in figure 5, revealing a clear asymmetry along the molecular axis. Through quantum scattering calculations, these characteristics were shown to originate from the interference among a small subset of partial waves, identifying thereby a final-state effect.

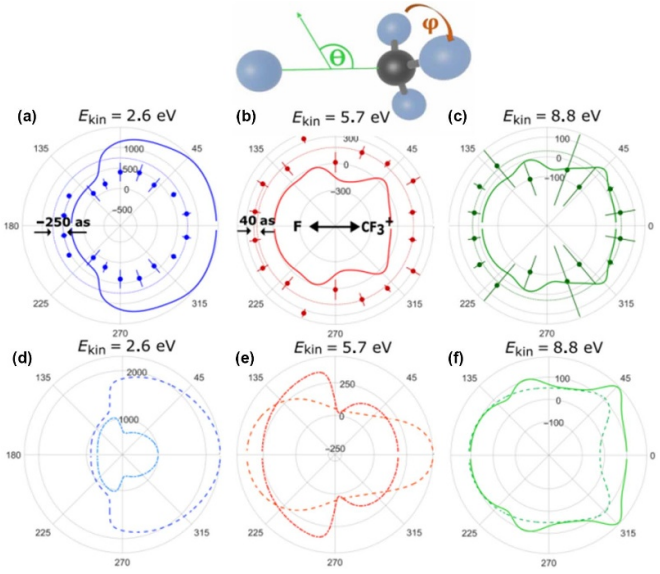

Figure 5. (a)–(c) Angle-resolved photoionization time delay with respect to argon in the recoil frame of the HOMO channel of CF_4 for (a) SB12, (b) SB14, (c) SB16. (d)–(f) Theoretical RABBITT delays for the partial-wave combinations of $l = 2 \sim 3$ (dash-dotted line), $l = 1 \sim 3$ (dashed line), $l = 1 \sim 4$ (thin line). From [56]. Reprinted with permission from AAAS.

A recent investigation [57] in 2022 delves into the asymmetry of attosecond photoionization time delays for NO in its molecular frame. In figure 6(a), the potential energy curve of NO illustrates the single-photon-induced ionization from the 4σ inner-valence shell, creating a $c^3\Pi$ ionic state that dissociates into the (N^+, O) channel through bond stretching. The recoil angle of the ionic fragments coincides with the bond orientation along N and O atoms, effectively defining the molecular frame [55]. The key findings are demonstrated in figure 6(b), highlighting the difference in the measured photoionization time delays between the emission of the photoelectron along the N/O end in the molecular frame, $\tau_{\mathrm{N-O}}^{\mathrm{MF}} = \tau_{\mathrm{N}}^{\mathrm{MF}} - \tau_{\mathrm{O}}^{\mathrm{MF}}$. A significant delay difference of 150 as is observed in the vicinity of the shape resonance around $E_e \approx 7.0$ eV, which aligns with *ab initio* simulations of the two-photon time delay. Furthermore, an asymmetric photoionization time delay up to 100 as between parallel and perpendicular transitions is evident, which arises because photoelectrons emitted perpendicular to the molecular axis experiences a π transition, suppressing the shape resonance effect.

In the same year, Ahmadi *et al* also reported on the emission-angle-resolved photoionization time delay of CF_4 in the recoil frame where CF_4 is orientated parallel and perpendicular to the laser polarization axis [58]. A local minimum for the case of parallel orientation was observed, while the time delay for the case of perpendicular orientation displayed a smooth variation. These results demonstrate that the anisotropic photoionization time delays encode the anisotropic nature of the molecular potential landscape, and indicate that

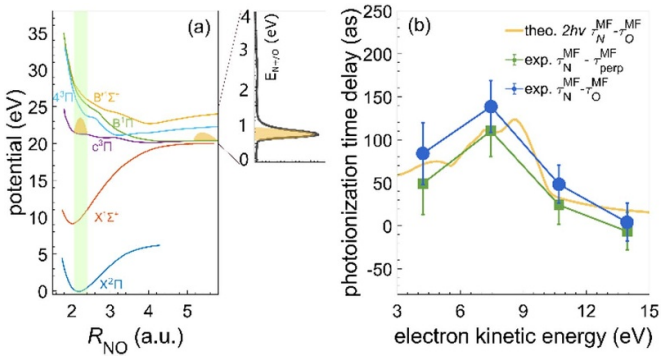

Figure 6. Orientation-dependent asymmetric molecular photoionization time delay. (a) Potential energy curve of the NO molecule. (b) Difference in the photoionization time delay as a function of the photoelectron energy. Reprinted figure with permission from [57], Copyright (2022) by the American Physical Society.

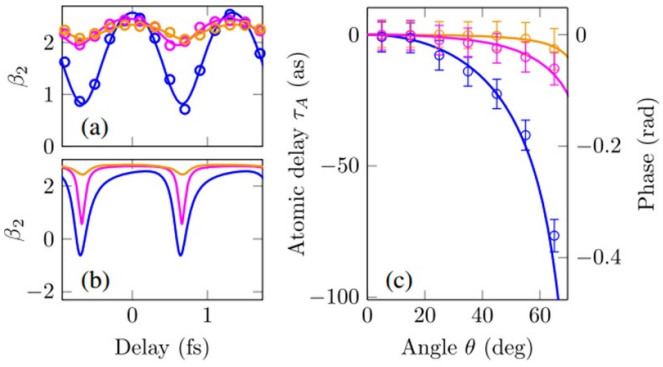

Figure 7. (a) Experimental and (b) theoretical anisotropy parameter β_2 as a function of time delay. (c) Angle-resolved atomic time delay for SBs 14, 20 and 22 for argon. Figure adapted from Ref [62]. Reprinted figure with permission from [62], Copyright (2019) by the American Physical Society.

the time delays in molecules cannot be simply decomposed into a sum of the EWS delay and the CC delay.

2.3. Angle-resolved time delay and partial wave reconstruction

Partial wave analysis is a powerful tool for uncovering the dynamics of attosecond photoelectron emission, with PADs acting as interference patterns [59]. In 2016, Heuser *et al* reported the first experimental observations of emission-angle-resolved two-photon time delays in helium as a function of the electron energy, using an AttoCOLTRIMS setup. A significant angular dependence was observed, with time delays rapidly decreasing as the emission angle deviated from the laser polarization axis by 50° [60].

The time-resolved PADs of photoelectrons ionized by linearly polarized photons can be decomposed using Legendre polynomials:

$$P(\theta,\tau) = \frac{\sigma_0}{4\pi}\left(1+\sum_{n=1}^{\infty}\beta_n(\tau)\,P_n(\cos\theta)\right).$$

Through this method, Cirelli *et al* extracted static and time-resolved anisotropy parameters β_n for argon, showing that autoionizing resonances could introduce anisotropy into angle-resolved time delays [61]. Similar findings were reported recently by Busto *et al*, as shown in figure 7 [62]. In this work, the angular variation of the time delay was explained by asymmetric contributions of absorption and emission pathways, following the Fano's propensity rule, which results in an incomplete interference among l-resolved partial waves.

The anisotropy coefficients $\beta_n(\tau)$, which describes the photoionization anisotropy, encode the relative amplitude and phase shift between partial waves populated through two-photon ionization. Time-resolved PAD measurements offer the opportunity to reconstruct the phase of each partial wave and the transition amplitude of a single scattering channel. In 2020, Fuchs *et al* reconstructed the energy-dependent CC time delay between s and d waves coupled to a single ionic state in helium [63]. In the same year, Joseph *et al* reported on the anisotropy parameters obtained from the RABBITT measurements of Ar and Ne [64]. The challenge of incoherent ionic states in these atoms, which adds to the difficulty in the reconstruction of partial wave information, was addressed in 2022 by Peschel *et al* [65], who extracted XUV-induced one-photon transition phases and amplitudes of $p \to d$ and $p \to s$ pathways in Ne. The time-resolved asymmetry analysis, previously applied to atomic systems, has been successfully extended to the acetylene molecule. The observed increase in the phase shift between $\beta_2(\tau)$ and $\beta_4(\tau)$ reflects a fundamental difference in shape between atomic and molecular systems [66].

In addition, advancing the complete formation of the photoelectron wave packet, Autuori *et al* have successfully reconstructed both the modulus and phase of the partial-wave amplitudes during two-photon ionization of helium using the spectrally and angularly resolved attosecond interferometry [67].

The general RABBITT scheme, with the NIR field polarized parallel to the XUV-APT, attributes the angle dependence of two-photon time delays to interference among partial waves with resolved l-quantum numbers [62]. A recent work proposed an atomic partial wave meter using a polarization-skewed (PS) NIR field [41]. By rotating the relative polarization axis of the XUV-APT and NIR lasers from a parallel to a perpendicular geometry, both the proportion and the two-photon phase shift of each partial wave are modulated, resulting in a skewed PAD and an asymmetric distribution of two-photon phase shifts. Figures 8(a)–(d) demonstrate the angle-resolved phase shift, defined as $\Delta\phi_{rel}^{\Theta_T} = \phi_0(\theta) - \phi_0(\Theta_T)$, as a function of the skewed angle between the XUV-APT and the NIR fields, Θ_T, for SB18 in helium. *Ab initio* theoretical simulation results, calculated using the R-matrix with time dependent (RMT) code [68–70], align well with the experimental observations.

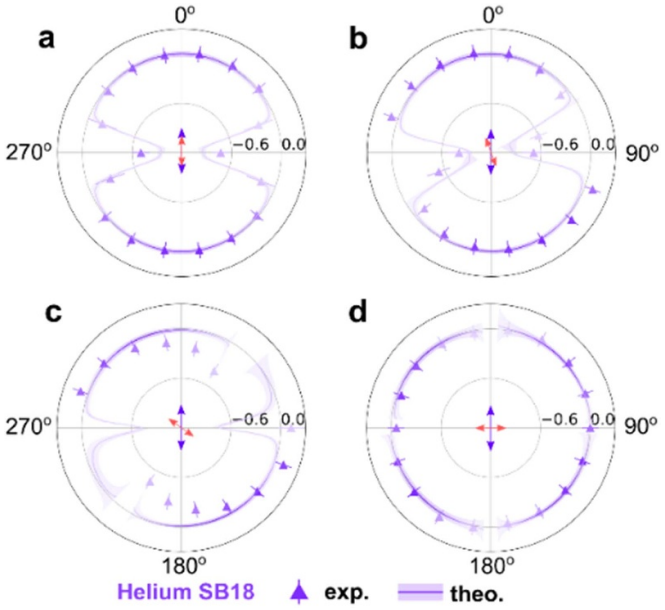

Figure 8. Emission angle-resolved atomic relative phase shift in helium at a skewed angle (a) $\Theta_T = 0^\circ$, (b) 20°, (c) 54.7°, and (d) 90°. Reproduced from [41], with permission from Springer Nature.

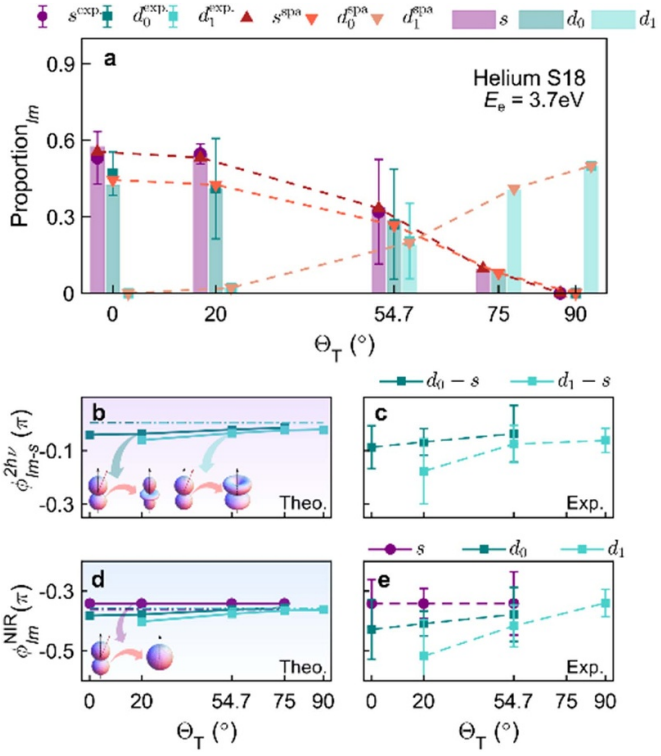

Figure 9. Full partial wave analysis of helium. (a) m-resolved partial wave proportion as a function of Θ_T. (b), (c) Partial wave phase shift difference between d and s waves from the RMT calculations and experimental reconstruction. (d), (e) m-resolved CC phase shifts from the (d) theory and (e) experiment. Reproduced from [41], with permission from Springer Nature.

A full partial wave analysis is performed to interpret the behavior of the skewed PADs and phase shift distributions. Figure 9 demonstrates the partial wave ratios (panel (a)) and relative two-photon phase shifts with respect to the s-wave (panels (b) and (c)) in helium as a function of Θ_T. The m-resolved partial-wave proportion and phase shift are reconstructed via complex fitting of measured PADs and $\Delta\phi_{rel}^{\Theta_T}$, employing partial wave decomposition:$P_{SB}(\theta,\varphi) = \Sigma_{l,m} c_{lm} Y_{lm}(\theta,\varphi)\, e^{-i\phi_{lm}^{2h\nu}}$. Theoretically, the two-photon phase shift and proportion of each partial wave are obtained with the RMT calculations by calculating PADs given by a specific partial wave. In addition, an analytical expression for the Θ_T-dependent partial wave proportion, derived using the soft-photon approximation [71], closely matches the numerical RMT results. The m-resolved CC phase shift is further displayed in figures 9(d) and (e), which is obtained by subtracting the one-photon phase shift for the $s \to p_0$ transition.

The polarization-controlled attosecond interferometer was later extended to resolve the interference of quantum transition pathways in neon [72]. With the NIR field polarized parallel and perpendicular to the XUV-APT, the emission-angle-resolved relative two-photon phase shifts in neon display a significant dependence in the photoelectron energy. As the SB order increases, the observed $\Delta\phi_{rel}^{SB}$ varies more slowly as θ deviates from the polarization axis of the NIR field. The reconstructed ionic-state-resolved partial wave phase shifts reveal that the energy dependence of $\Delta\phi_{rel}^{SB}$ is due to the decreasing relative phase shifts among different partial waves. Moreover, the two-photon phase shift of the p wave coupled to the P_0 ionic state displays a significant symmetry and energy dependence. In neon atoms, it is populated through the interference between the $p \to d \to p$ and $p \to s \to p$ pathways. Given the analytical expression for the interference of these transition pathways and considering that the two-photon phase shift of a single pathway is independent of the magnetic quantum number in the perturbative regime, the relative ratio of the radial amplitudes between $p \to d \to p$ and $p \to s \to p$, and their individual phase shifts can be reconstructed. In this scenario, the polarization axis of the NIR field serves as a phase controller. This results in destructive interference at $\Theta_T = 0^\circ$ and constructive interference at $\Theta_T = 90^\circ$.

Further changing the laser field geometry, RABBITT measurements with a circularly polarized XUV-APT have provided new insights into the phase response of circular dichroism of chiral targets [73]. In addition, comparisons between two-photon phase shifts with co-rotating and counter-rotating XUV-APT and NIR fields have been used to separate partial-wave-resolved EWS delays and CC delays in helium atoms as a function of photoelectron energy [74].

As an extension to the RABBITT technique that considers the pure two-photon transitions, more recently, Bharti *et al* proposed a '3-SB' scheme where the XUV-APT with an energy interval of $4\omega_{NIR}$ is generated by the second harmonic of the fundamental near-infrared field. Thus three SBs are generated between two mainbands, where the lower and higher ones are resulting from the interference between two- and four-photon transition pathways, and the middle ones are

generated from three-photon transitions [75, 76]. This scheme indicates that the measurement of photoemission time delay can be further advanced into the few-photon regime. In this case, the distinction of the high-order transitions and detection of the contributions from high-order partial waves are necessary to comprehend the underlying physics.

3. Photoionization delay in multi-photon regime

Compared with the single-photon ionization time delay, it is predicted theoretically [77] that there is an attosecond-level photoabsorption time delay during the resonant two-photon ionization process of helium atoms. In this process, the photoelectron may stay at the resonant excited state for a brief period before absorbing another photon to get ionized.

3.1. Delay in freeman resonance

In 1987, Freeman *et al* [78] experimentally observed multiphoton resonance ionization. During the process of multiphoton ionization in intense laser fields, the laser field induces a Stark shift in the energy level of the highly excited Rydberg state, potentially leading to resonant multiphoton ionization. The Freeman resonance makes thus an ideal system to testify the theoretical prediction of a resonant photoabsorption time delay. In quantum mechanics, time is not directly observable; instead, time information is extracted by measuring phase. Based on two-dimensional field manipulation, the attosecond residence time of electrons in different resonance states during the multiphoton absorption process has been measured [79].

As depicted in figure 10, employing a phase-controlled orthogonal two-color (OTC) laser field [80–82], argon atoms coherently absorb six 400 nm photons reaching resonance with $4f$ and $5p$ states, followed by the absorption of one photon transiting to the continuum state. By employing electron–ion coincident measurements to accurately measure the spatiotemporally resolved PAD as a function of the relative phase ϕ_{L} of the OTC field, a phase delay of 0.21π between the $4f$ and $5p$ electrons was identified, corresponding to a resonant ionization delay of 140 as. This experimental detection technique is versatile and applicable to various targets. By correlating the laser phase with the measured PAD, the attosecond ionization delay of electrons in the multi-photon absorption process can be accurately determined.

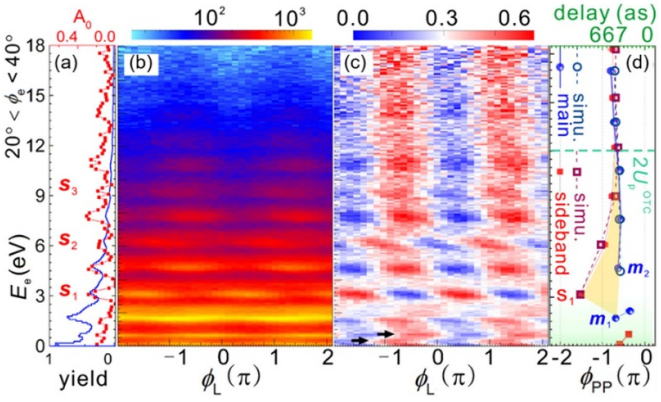

Figure 10. Freeman resonance ionization delay in Ar. (a) Measured photoelectron energy spectrum. (b) Measured and (c) normalized photoelectron energy spectra as a function of the relative phase ϕ_L of the OTC field. (d) Energy-resolved photoelectron emission phase shift. Reprinted figure with permission from [79], Copyright (2019) by the American Physical Society.

employing ultrafast laser pulses to interact with ArKr dimers [84, 85]. A linearly polarized pump laser is used to produce the $ArKr^+$ ion, and an elliptically polarized laser pulse probes the electron tunneling from $ArKr^+$. Figure 11(a) illustrates the measured photoelectron momentum distribution (PMD) of double ionization from ArKr in the polarization plane. The linearly polarized pump pulse ionizes electrons from the Kr side, leading to a PMD concentrated along the z-axis with $|pz_e| \leqslant 0.2$ a.u. Due to the angular streaking effect of the probe pulse [26–28], the elliptically polarized probe pulse mainly ionizes electrons from the Ar side with a momentum $|pz_e| \geqslant 0.2$ a.u. By selecting a specific molecular axis direction, the PMD ionized by the probe pulse is shown in figure 11(b). As presented in figure 11(c), the measured and simulated PADs exhibit two deflection peaks at $-54°$ and $-122°$, corresponding to resonant and direct ionization channels, respectively. Here, the simulation employed the improved Coulomb-corrected strong-field approximation [86–88].

Direct ionization involves electrons tunneling out of the barrier from the Ar side directly under influence of the pump laser pulse. In the scenario of resonance ionization, on the other hand, electrons may pass through the internal barrier between Ar and Kr^+, become trapped in the molecular potential well of Kr^+ to form a transient state [79, 88], and eventually get released to the continuum after the end of the laser field. By employing direct tunneling ionization as a self-reference arm of the attoclock, the time delay of the electrons trapped in the resonant state is determined to be around 3.5 fs. These findings unveil the semiclassical representation of transient resonance ionization in diatomic systems. The proposed self-reference molecular attoclock technique and theoretical model offer a new technical approach to exploring ultrafast electron dynamics in complex molecular systems.

3.2. Resonant photoionization delay

Over the past two decades, researchers have developed a variety of attosecond interrogation techniques [20], including the attoclock technique for timing multiphoton and tunneling ionization [26–28].

Recently, a novel approach to measuring the resonance photoionization time delay of $ArKr^+$ using a self-reference asymmetric molecular attoclock has been proposed [83],

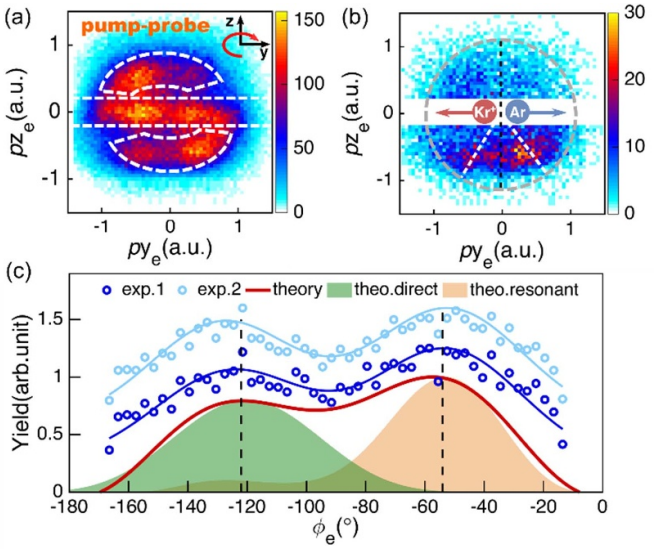

Figure 11. (a) Measured PMD in the polarization plane of ArKr from double ionization. (b) Measured PMD ionized by the probe pulse with $ArKr^+$ oriented as sketched in the inset. (c) PADs from experimental measurement and theoretical simulation. Reprinted figure with permission from [83], Copyright (2022) by the American Physical Society.

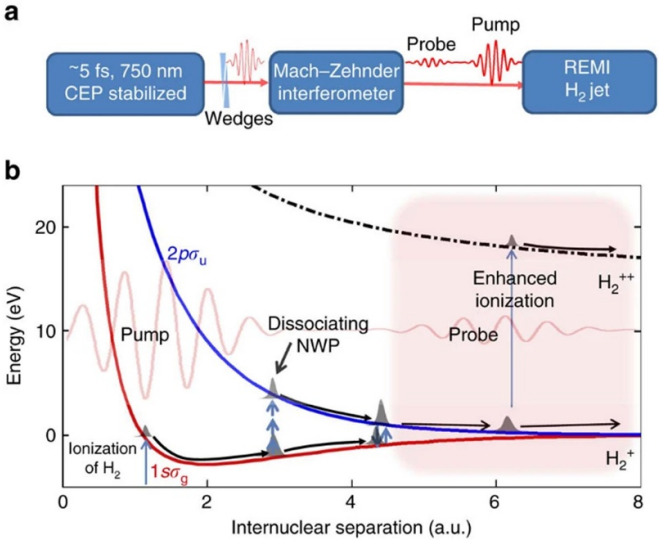

Figure 12. (a) Experimental scheme of generating few-cycle pump–probe laser pulses, which were used to clock ultrafast dynamics in H_2. (b) An intuitive picture describing the interaction between a pair of few-cycle laser pulses and the hydrogen molecule. The pump pulse ionizes H_2 and excites the cation H_2^+. The probe pulse steers the electron motion with a scanning time delay to observe the whole electron localization process. Reproduced from [91], with permission from Springer Nature.

4. Timing and control using ultrafast stopwatch

In the realm of XUV-initiated photochemical processes, molecular dynamics are typically explored via interferometry in the frequency domain, reflected as the perturbative processes involving absorption and emission of photons. The construction of temporally tailored laser fields has opened up the possibility to observe and control molecular dynamics in the time domain, an emerging field known as optochemistry. In this scenario, the dynamics of electrons and nuclei within a molecule are mainly driven by these tailored laser fields, whose optical field characteristic dominates laser-molecule interactions.

Direct observation of nuclear dynamics can be realized using a conventional pump–probe scheme with two femtosecond laser pulses. However, it is difficult to trace the sub-femtosecond nuclear and electronic dynamics due to the limitation of temporal resolution of multicycle laser pulses. Scientists have developed various approaches to observe and clock the ultrafast dynamics in molecules, taking advantage of different physical processes such as the evolution of electronic, vibrational and rotational wave packets. These approaches can be categorized as different types of ultrafast stopwatches, each with distinct advantages.

4.1. Few-cycle pump–probe scheme for tracing ultrafast dynamics

An intuitive approach to timing ultrafast dynamics involves generating and using increasingly shorter laser pulses, forming a few-cycle pump–probe scheme as a direct extension of the conventional multicycle one. This approach provides sub-femtosecond temporal resolution and enables real-time observation of wave-packet evolution in small molecules. After the pump pulse initiates the ionization process, a probe pulse with a scanning time delay monitors subsequent molecular dynamics.

When an electron is removed upon interaction with a strong ultrashort laser pulse, the initial nuclear wave packet evolves along the potential energy curves of the cation. The field-free evolution of the nuclear wave packet is interpreted through coherent interference of vibrational and rotational eigenstates. The resulting collapse and revival of the nuclear wave packet can be observed using the few-cycle pump–probe scheme scanning with an extended span of time delay [89].

The transition between electronic states is involved considering laser-molecule interaction following ionization. Thereby, the few-cycle pump–probe scheme can also clock ultrafast electron dynamics, as illustrated in figure 12, where electron localization occurs by superimposing two degenerated eigenstates with opposite parities [90]. The internuclear distance and time information for electron localization are recorded by few-cycle laser pulses [91], providing insights into the role of electron dynamics in driving chemical reactions.

In contrast to tunneling induced by a strong laser pulse, there is a certain possibility for the electron to be trapped in a Rydberg state, termed as frustrated tunnelling [92]. This Rydberg excitation process can also be tracked in real time using the aforementioned approach, where the few-cycle probe laser pulse triggers the Rydberg excitation. Three distinct internuclear distances were recognized to enhance excitation [93], proving the existence of multiphoton resonant excitation.

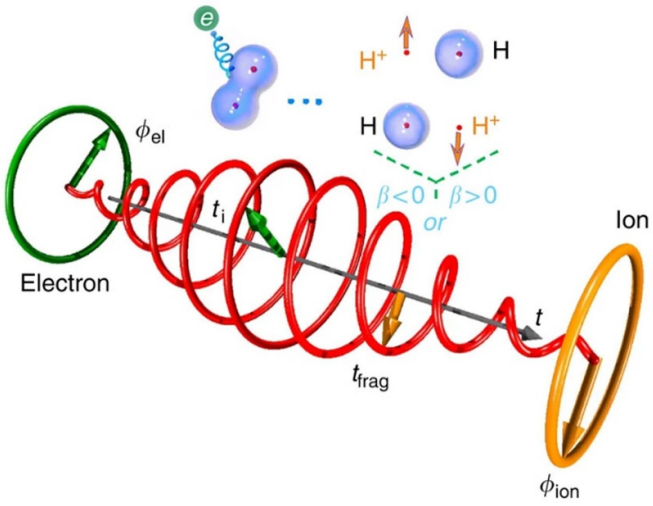

Figure 13. A general scheme of encoding ionization instant and fragmentation (or excitation) instant into the photoelectron and ion angular distributions via a circularly (or elliptically) polarized laser pulse. Reproduced from [99], with permission from Springer Nature.

4.2. Angular streaking scheme via circular polarization

Advancements in the few-cycle pump–probe scheme have opened up new possibilities for clocking the ultrafast dynamics from rotation and vibration of nuclei to even faster electron excitation. However, this comes with a trade-off: enhanced temporal resolution results in reduced energy resolution, leading to the broad frequency or energy spectra.

An alternative route to achieving sub-femtosecond or even attosecond temporal resolution is the attoclock technique [26–28], which uses angular streaking with a circularly or elliptically polarized laser pulse. The rotating electric vector works as a spinning clock, providing time information for various ultrafast processes.

The angular streaking technique has been widely used to resolve field-driven ionization processes. For example, a number of works have utilized angular streaking to resolve the tunneling time delay [20, 26, 27, 94], which has remained controversial since the birth of quantum mechanics. In the context of time resolution using angular streaking, however, the consensus now is that tunneling ionization is near instantaneous [20] although the observed tunneling delay could be slightly negative due to under-barrier recollision [95]when the laser strength is high enough such that ionization occurs in the near over-barrier regime instead of in the deep tunneling regime. In addition to tunneling delay, the time delay between sequential double ionization has been probed using an elliptically polarization laser pulse [96–98].

Furthermore, Coincidence measurements of electrons and ions can provide more information, such as the phase associated with the nuclear wave packet. As shown in figure 13, the instantaneous polarization information is encoded into the asymmetric emission of electrons in the molecular frame, leading to electron localization driven by even a symmetric laser field, which can be observed via angular streaking [99].

For nuclear fragments, the rotation of diatomic molecules serves as clock hands for timing bond-stretching dynamics. The field-free evolution of rotational eigenstates provides different timelines that interfere with each other and are probed by subsequent laser pulses, allowing deduction of time information for various molecular dynamics from the shape of the superimposed rotational wave packet [100].

4.3. Ultrafast stopwatch via shaped-polarization

Phase-controlled asymmetric femtosecond laser fields have been utilized to steer bound electrons within a molecule, leading to controlled molecular bond breaking [90, 101–104]. This progress represents a significant step toward coherent control of chemical reaction dynamics. For instance, phase- and polarization-controlled two-color laser fields have been employed to realize two-dimensional electron localization within a molecule, leading to controlled bond breaking and subsequent chemical reactions [93, 105–107].

Recently, a novel scheme of an ultrafast stopwatch [108] has been proposed, through the implementation of a PS laser pulse, and its powerful and robust applicability in probing and controlling molecular dynamics in strong laser fields has been demonstrated. The rotating polarization vector of the PS laser pulse induces unidirectional rotational motion in molecules [109–113]. Furthermore, the PS laser pulse exhibits a unique capability to resolve ultrafast dynamics across neighbouring optical cycles, distinguishing it from linearly or circularly polarized counterparts, including the attoclock technique.

4.3.1. Clocking above-threshold double ionization of molecules. Dissociative above-threshold double ionization of molecules involves both chemical bond breaking and the release of two electrons. The former may yield abundant information from the measured kinetic energy release (KER) spectrum of the nuclear fragments, while the latter could serve as the two arms of the ultrafast stopwatch [114].

The KER spectrum can be used to infer the critical internuclear distances where enhanced ionization occurs, from which two distinct scenarios were proposed. One is the charge-resonance-enhanced ionization [115, 116] in the tunnelling regime, where the localized electron around the up-field nucleus experiences enhanced ionization. The other is above-threshold Coulomb explosion [117, 118] in the multi-photon regime, where the electron populated at the ground state undergoes multi-photon resonant transition and is subsequently released into the continuum.

Various photon-number-resolved dissociation pathways are identified from the multi-peak KER spectrum, labeled by the number of photons absorbed during the process of bond stretching and subsequent secondary ionization [114]. Gating distinct peaks on the KER spectrum allows us to obtain the corresponding momentum distributions of the two released electrons, where a typical example is shown in figure 14.

The two electrons released at different instants in a PS laser pulse sequentially emit in distinct directions, leading to an X-shaped structure. The crossing angle of the X-shaped structure

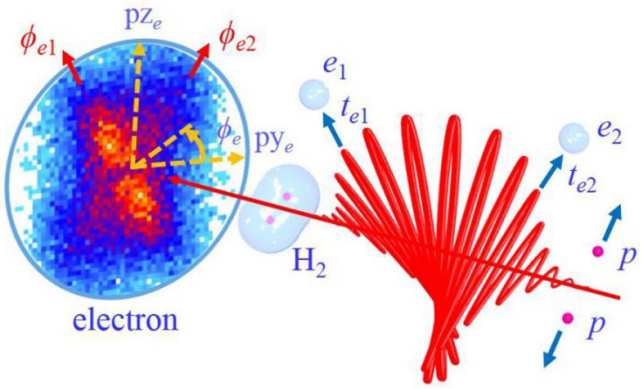

Figure 14. Schematic illustration of the ultrafast stopwatch using a PS laser pulse to clock the dissociative above-threshold double ionization of H_2. Two electrons sequentially released at different instants are angularly streaked to different emission directions by the PS laser pulse, leading to an X-shaped PMD. Reprinted figure with permission from [114], Copyright (2021) by the American Physical Society.

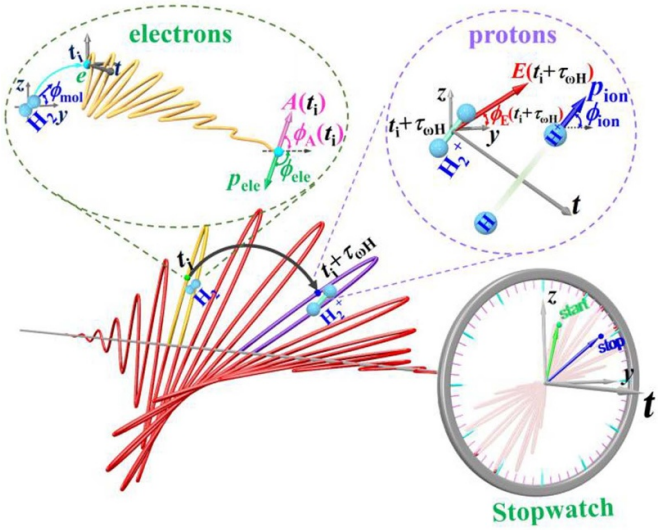

Figure 15. Sketch of the ultrafast stopwatch using a PS laser pulse to probe the bond-stretching time of H_2. Reprinted figure with permission from [108], Copyright (2019) by the American Physical Society.

encodes the bond-stretching time of the dissociative above-threshold double ionization. Thus, one can obtain the time interval between two ionization steps by converting the emission directions into ionization instants with respect to the spatiotemporal profile of the PS laser pulse.

4.3.2. Probing bond-stretching time of molecules. In the case of dissociative single ionization of molecules, the measurement is limited to one electron and the associated nuclear fragments. Consequently, the emission directions of electrons and nuclear fragments serve as the two arms of the ultrafast stopwatch [108]. As depicted in figure 15, the electron released at a specific instant undergoes oscillation driven by the remaining laser field. The final momentum of the electron can be utilized to determine the ionization instant. Meanwhile, the momentum distribution of the nuclear fragments can also be used to deduce the photoabsorption instant during the bond stretching, as the dipole transition rate strongly depends on the strength and orientation of the instantaneous laser field.

The aforementioned method is only applicable to the well-known one-photon and net-two-photon dissociation pathways, since the photon number involved in the bond-stretching process needs to be known in advance. To circumvent this issue, an alternative timing method has been proposed that promptly provides the bond-stretching time and photon number involved within the molecular frame [119]. The deflection angle encodes the bond-stretching time between the ionization instant and the photon-coupled dipole-transition instant, while the half-width of the molecular-frame PADs encodes the photon number absorbed and emitted during the laser-molecule interaction. This approach contributes to a deeper understanding of light-induced bond breaking and formation in both temporal and energy dimensions.

4.3.3. Controlling parallel and perpendicular transitions in molecules. For linear molecules, laser-molecule interactions depend on the crossing angle between the laser polarization and molecular orientation, leading to two distinct dipole transitions. One is the parallel transition where the laser polarization is favored parallel to the molecular orientation and induces transition between two molecular orbitals with $\Delta\lambda = 0$, where λ denotes the orbital angular momentum projected along the molecular orientation. The other is the perpendicular transition where the laser polarization is favored perpendicular to the molecular orientation and induces transition between two orbitals with $\Delta\lambda = \pm 1$.

In the PS laser pulse, the polarization vector rotates from cycle to cycle. Consequently, for a molecule with its orientation nearly parallel to the polarization direction at the leading edge, it will sequentially undergo the parallel transition at the leading edge and perpendicular transition at the falling edge, as shown in figure 16.

The inset of figure 16 illustrates the measured momentum distribution of nuclear fragments resulting from the dissociative (single and double) ionization of H_2 driven by a tailored PS laser pulse. Nuclear fragments emitting along the vertical direction originate from a parallel molecular reaction pathway, while those emitting along the direction of 165° stem from a hybrid reaction pathway involving both parallel and perpendicular transitions.

The molecular reaction pathway can be further manipulated via adjusting the time-dependent polarization waveform of the PS laser pulse. A half-wave plate is used to control the incident polarization direction before the multi-order wave plate, so that the leading and falling edge of the PS laser pulse can be precisely adjusted. Thereby, the parallel and perpendicular reaction pathways can be controlled as designed.

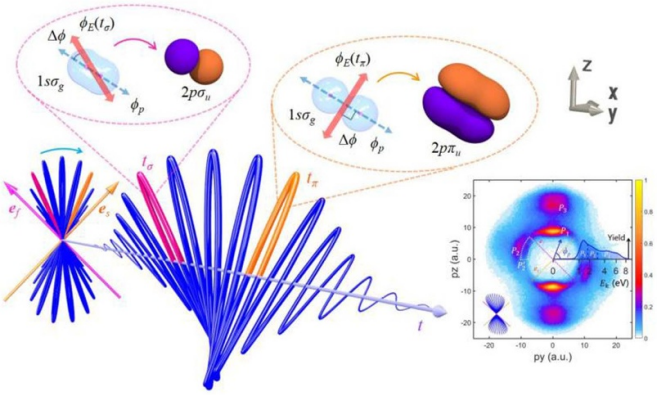

Figure 16. Sketch of the ultrafast stopwatch using a PS laser pulse to induce parallel and perpendicular transitions in H_2. The measured momentum distribution of the nuclear fragments are shown as the inset. Reprinted figure with permission from [120], Copyright (2023) by the American Physical Society.

5. Probe and control of bimolecular reactions

Beyond molecular bond breaking, laser-molecule interaction can give rise to molecular reactions involving bond formation processes. Numerous studies have delved into the formation of new chemical bonds during the interplay of light and molecules, with a specific emphasis on the photo-induced fragmentation of molecules. For instance, the dissociation of a water (H_2O) molecule induced by light can lead to the creation of hydrogen (H_2), accompanied by the breaking of O–H bonds and the formation of H–H bonds [121–123]. The time-resolved fragmentation of an SO_2 molecule, resulting in the formation of an O_2 molecule, has also been investigated under the influence of intense femtosecond laser pulses [124]. The reaction processes in these studies typically involve the decomposition or rearrangement of a single molecule, which is named as unimolecular reactions. The unimolecular reactions, involving ultrafast intramolecular bond cleavage and formation processes, can be further controlled by steering the nuclear vibrational, rotational, and dissociation motions and even electronic motions within the molecule by using tailored laser pulses. By tailoring the laser parameters (including intensity, pulse duration, frequency, polarization, phase, etc) to match the specific energy levels and dynamics of the molecules through coherent excitation, the bond formation and cleavage in the chemical reactions can be controlled in a desired way.

5.1. Experimental realization of bimolecular reactions

In comparison to unimolecular reactions, the bimolecular reactions involving intermolecular interactions are much more general chemical reaction processes in nature. The molecule–molecule interactions can also lead to the breaking of old bonds and formation of new bonds among the molecules, where the involved processes occur on the picosecond or femtosecond time scale. Traditional approaches for investigating bimolecular reactions have relied on beam scattering measurements [125–130], aiming to collect information including product kinetic energy, angular distribution, reaction rate coefficients, and state-selective cross-sections. However, these measurements face experimental hurdles in accurately determining the reaction time zero and the initial internuclear distance between the two reacting molecules. Consequently, the detailed understanding of the mechanisms and dynamics of bimolecular reaction processes has been significantly impeded.

The experimental approach of initiating light-induced bimolecular reactions starting from molecular dimers provides a clear time trigger and a predetermined starting internuclear distance for the reaction. The study of photo-induced bimolecular reactions, starting from a van der Waals dimer, has been pioneered by Witting's and Zewail's groups. For instance, in [131], Witting and co-workers employed the CO_2–HBr dimer to study the oriented chemical reaction. In [132] by Scherer *et al*, pump–probe study was performed to clock the bimolecular reaction starting from the HI-CO_2 dimer based on the laser-induced fluorescence technique. Since the dimer systems have well-defined equilibrium geometries, the starting point of the light-driven bimolecular reaction can be precisely tracked in spatial and time domains. This has further permitted the study of the ultrafast dynamics of bimolecular reaction using femtosecond pump–probe technique and the coherent control using tailored laser fields.

Recent studies [133, 134] have explored the ultrafast dynamics of light-driven bimolecular reactions leading to the formation of trihydrogen cations H_3^+ and its isotope D_3^+ from the hydrogen dimer (see figures 17 and 18). This reaction, also known as the Hogness and Lunn reaction [135], plays a pivotal role as the initiator for numerous chemical reactions in interstellar clouds [136, 137]. It has been extensively studied in the past in the context of unimolecular reactions [127, 128, 138–148], where the formation dynamics of the trihydrogen cation from an organic carbohydrate can be visualized since an unambiguous time trigger of the reaction is clearly identified. While these studies offer ample insights to enhance our comprehension of the formation kinetics of trihydrogen cations resulting from the fragmentation of sizable organic compounds, a more pertinent concern within interstellar clouds would involve generating H_3^+ or D_3^+ from molecule–molecule interaction.

Through femtosecond pump–probe measurements, researchers have probed and characterized the ultrafast formation dynamics of D_3^+ in the light-driven bimolecular reaction within a D_2–D_2 dimer [133, 134]. The reactions were initiated by an ultrashort pump pulse that ionized one or both molecules in the dimer, followed by a later-arriving ultrashort probe pulse to monitor the progress of the bimolecular reaction. Leveraging the reaction microscope, ion fragments resulting from the same dimer reaction can be detected in coincidence, allowing for the identification of different reaction channels leading to the formation of D_3^+. It was observed [133] that the formation time of D_3^+ varied for different pathways, with a fast double-ionization pathway occurring within 35 fs and a slow single-ionization pathway taking approximately 139 fs. Additionally, by utilizing a tailored linearly polarized two-color laser pulse with a directional asymmetry (scheme 2 in figure 18) during the dissociative ionization

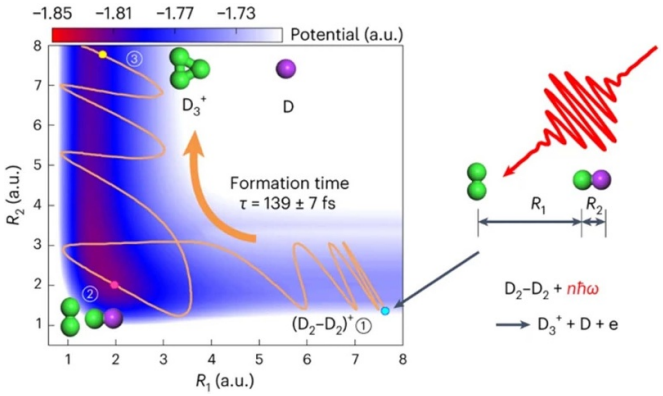

Figure 17. Light-driven formation of D_3^+ in bimolecular reactions starting from a D_2–D_2 dimer. Reproduced from [133], with permission from Springer Nature.

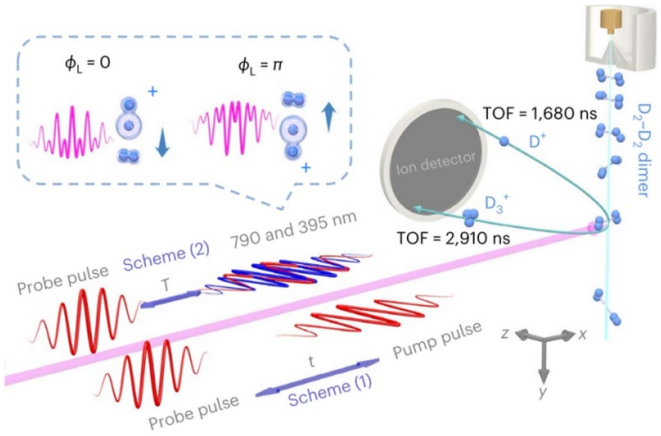

Figure 18. Two sets of pump–probe schemes implemented in studying the bimolecular reaction of the D_2–D_2 dimer. Reproduced from [133], with permission from Springer Nature.

of one of the D_2 molecules in the dimer, it is demonstrated [133] that the direction in which D_3^+ ions are ejected in the double ionization pathway (D^+, D_3^+) can be controlled by tuning the relative phase of the two-color laser fields, thereby achieving attosecond-level precision control over chemical reactions. The observation that D_3^+ and D^+ are expelled in opposite directions supports the idea that the neutral atom needs to be oriented towards D_2^+ for the successful production of D_3^+. More recently, using a modified pump–probe scheme, where the pump pulse induces nonadiabatic alignment of D_2 molecule and the probe pulse excites the D_3^+ formation, it is demonstrated that the sterodynamical control of D_3^+ formation from the bimolecular reaction in the D_2–D_2 dimer can be achieved [149]. Such sterodynamical control of strong-field molecular dynamics is different from that reported in the crossed molecular beam studies [150, 151], where the stereodynamical control of strong-field molecular dynamics relies on the alignment-dependent photodissociation rather than the relative orientation of the two collision reactants.

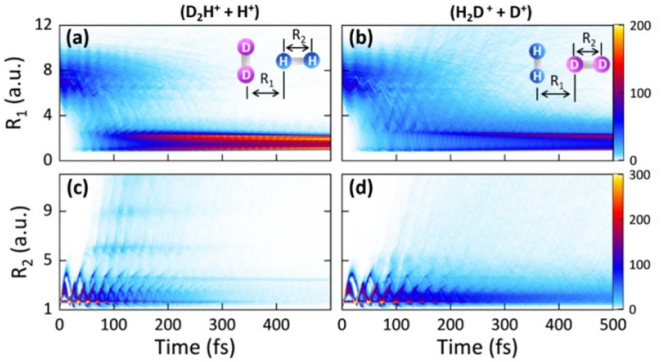

Figure 19. Evolution of reaction coordinates of (a), (b) approaching distance R_1, and (c), (d) departing distance R_2 in the molecular dynamics simulations for the formation of (a), (c) (D_2H^+, H^+) and (b), (d) (H_2D^+, D^+) channels from the bimolecular reaction of the H_2–D_2 dimer with initial T-shape configuration. Reprinted figure with permission from [152], Copyright (2024) by the American Physical Society.

By examining the H_2–D_2 dimer instead, one can gain insights into the kinetic isotope effect in bimolecular reaction dynamics. In a recent study [152], femtosecond pump–probe experiments with D_2–H_2 dimers have shed light on how nuclear vibrational motion significantly impacts reaction yield rates, efficiencies, and the dynamics of product formation in these reactions. When comparing the (D_2H^+, H^+) and (H_2D^+, D^+) reaction channels, a pronounced yield ratio of 1:1.6 was observed between the H_2D^+ and D_2H^+ channels, with D_2H^+ forming more rapidly than H_2D^+. Figure 19 illustrates the time-dependent changes in the approaching distance R_1 and the departing distance R_2 for the calculated reaction trajectories of both D_2H^+ and H_2D^+ formation channels. It demonstrates that the quicker vibrational motion of H_2^+ post single ionization within the dimer is responsible for this disparity, thus discovering a time-resolved kinetic isotope effect in bimolecular reactions. These findings have enriched our comprehension of the kinetic isotope effect in chemical reactions and paved the way for the coherent manipulation of reaction rates and outcomes in bimolecular reactions by sculpting the nuclear motions of the reacting molecules using light fields.

The technique of timing and controlling bimolecular reaction has been further applied to a heteromolecular dimer, H_2–CO [153], where the formation of the C–H bond is observed in the bimolecular reaction of two inorganic molecules. A tailored two-color laser field is employed not only to identify the formation of HCO^+ ion containing the C–H bond but also to realize the coherent control of the reaction dynamics. The ultrafast formation time for the C–H bond is determined to be approximately 200 fs. The real-time visualization and coherent control of the dynamics shed light on the most fundamental inorganic bimolecular reaction occurring in the interstellar clouds responsible for the C–H bond formation that produces organic molecules, paving the route towards the real-time visualization and coherent control over the dynamics with unprecedented precision.

5.2. Numerical simulation of bimolecular reactions

Theoretical calculations of the bimolecular reaction are usually based on molecular dynamics simulations employing the classical-trajectory Monte Carlo (CTMC) method. The first step of the molecular dynamics calculations is typically the computation of the PES of the specific bimolecular reaction channel. In the investigation of the reaction dynamics of D_3^+ formation [133], simulations were conducted starting with the T-shape configuration, where two molecular axes are perpendicular to each other. This T-shape configuration corresponds to the most stable equilibrium geometry since it has the lowest energy.

Figure 17 shows a typical reaction trajectory starting close to the equilibrium with zero initial velocity and an artificially frozen T-shape geometry. By defining two reaction coordinates of R_1 and R_2, the PES of the T-type cationic $(D_2–D_2)^+$ dimer is calculated as shown in figure 17. The formation of D_3^+ can be divided into three steps. Upon Franck–Condon excitation, the cationic state initially around the equilibrium geometry of the neutral state is populated. Under the force field of the cationic state, the D_2^+ ion starts to vibrate around the new equilibrium internuclear distance of 2.0 a.u. while moving to approach the neighbouring D_2 molecule, forming a D_4^+ compound in step 2. The D_3^+ ion finally formed when the neutral D atom departs away at a longer time delay, denoted as step 3.

An alternative approach to simulate bimolecular reactions is via an on-the-fly nonadiabatic molecular dynamics simulation. In this approach, the PES does not have to be computed beforehand. Rather, at each temporal step, the electronic structure and force field is computed on-the-fly, which in turn steers the nuclear motion. This approach enables the calculations of bimolecular reactions starting from different initial geometric configuration (see figure 20), neither does it restrict the symmetry and the geometry of the nuclear coordinates during the reaction. It has been appplied to account for various initial structural configurations. It has been shown that the formation time of D_3^+ strongly relies on its initial structural configuration. The average formation time after considering the contributions from all shapes was 150 fs, well in agreement with the timescale of the experimental value.

Besides, diverse theoretical approaches for numerically simulating bimolecular reaction dynamics were systematically surveyed, based on the formation of D_3^+ originating from the $D_2–D_2$ dimer [154]. Focusing on the principal coordinates relevant to this reaction shown in figure 20, PESs were constructed through first-principle quantum chemical calculations for each configuration. In addition to evolving classical trajectories on these PESs, the nuclear wave packet were also propagated on them by numerically solving the time-dependent Schrödinger equation, offering a quantum perspective on reaction dynamics. Several other approaches, such as the virtual detector method [155–158], Bohmian mechanics [159, 160] and backpropagation [20, 161–163], which includes the quantum effects to different levels, were used to extract effective information contained within the time-dependent nuclear wave packet for comparison. These methods yield similar

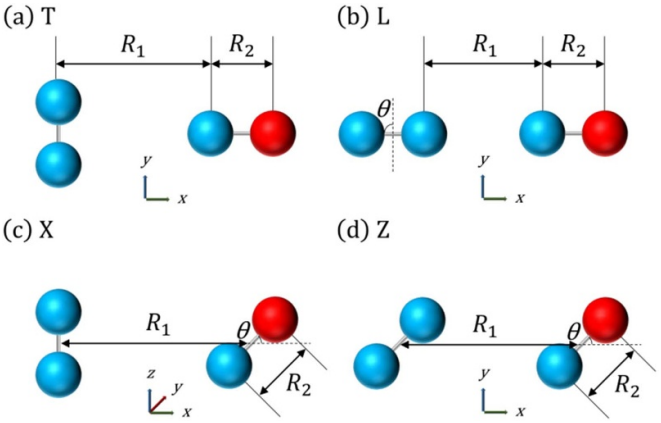

Figure 20. Different initial configurations and the respective reaction coordinates of the $D_2–D_2$ dimer. Reprinted figure with permission from [154], Copyright (2024) by the American Physical Society.

timescales, affirming their reliability. It also demonstrates the limited influence of quantum effects on nuclear motion and the general applicability of both classical and quantum methods in bimolecular reaction.

The possible influence of a distribution of initial nuclear momentum on the molecular dynamics were also explored, which were assumed to be zero before. Based on a reduced-dimensional Wigner quasiprobability distribution calculated by the nuclear wave function of the neutral $D_2–D_2$ dimer, CTMC simulations were carried out to extract the formation time distribution with the initial momentum of trajectories no longer simply zero. It is found that the most probable reaction time is close to that obtained by CTMC simulations with zero initial velocity, indicating that the initial distribution of nuclear momentum has only minor influences on the subsequent molecular dynamics. These theoretical studies on ultrafast bimolecular reactions not only enhances the understanding of detailed molecular dynamics but also lays the foundation for future studies, promising deeper insights into intricate quantum processes guiding chemical reactions.

6. Summary and perspective

This Topic Review covers recent advancements in the timing and control of ultrafast molecular dynamics with attosecond time resolution/precision, shaped by the continuous evolution of laser and detection technologies. From single-photon to multi-photon regimes, the investigation spans processes initiated by both XUV and NIR pulses.

The photoionization time delays, particularly in molecular frames, provides detailed insights into the fundamental interactions between light and molecules, capable of revealing tiny differences and asymmetries in the molecular potential landscape. It is made possible by a marriage between the attosecond metrology and the coincident detection capability. An atomic partial wave meter is further developed based on PS

laser pulses to single out individual contributions of different partial waves to the photoionization time delay.

The exploration extends into multi-photon resonance ionization processes, elucidating phenomena like Freeman resonance and resonant photoionization delay. Constructing a self-reference molecular attoclock, the delay of transiently trapped electrons in the $ArKr^+$ complex relative to those released directly can be determined to be on the level of a few femtoseconds with attosecond time precision.

The timing and control of molecular dynamics using temporally tailored laser pulses emerge as a key element. The development of an ultrafast stopwatch, especially through the implementation of PS laser pulses, is promising in probing and controlling molecular reactions. It features capabilities of resolving ultrafast dynamics beyond a single cycle, a characteristics distinct from the attoclock technique. From clocking above-threshold double ionization to probing bond-stretching times and controlling parallel and perpendicular transitions, the precision achieved opens new avenues for optochemical studies.

The culmination of these advancements is evident in the exploration of bimolecular reactions initiated within molecular dimers. The sophisticated femtosecond pump–probe measurements, together with the well-defined spatial starting point offered by dimer targets, reveal the dynamics of light-driven bimolecular reactions, shedding light on the formation of trihydrogen cations and their isotopes. The directional control achieved in the double ionization pathway further adds to our understanding of the control of bimolecular reaction processes.

In summary, this Topical Review captures a certain scope of research in ultrafast molecular dynamics, emphasizing the role of tailored laser pulses in unraveling and controlling the intricate light-molecule interactions. The achievements outlined pave the way for future investigations, promising continued revelations in the understanding and control of ultrafast molecular processes.

Looking ahead, the future of exploring how light interacts with molecules is full of exciting possibilities. The investigation of photoionization time delays in molecules is still in its exploratory stage, with most reports limited to small molecules. Interesting questions remain, such as the time scale of strong electron–nuclear correlation effects where the Born-Oppenheimer approximation breaks down, the chiral responds in the time domain, and the influence of attosecond electronic dynamics on chemical and biological reactions. Directly answering these questions from experimental measurements faces challenges in improving detection efficiency and energy resolution. Coincidence measurements involving high-repetition laser systems may help address these issues. Additionally, an improved theoretical description that accounts for nuclear–electron and electron–electron correlations is needed to discover and understand new physical mechanisms. Moreover, for molecules, especially large ones, the angular momentum is no longer conserved. Whether it makes sense to carry out partial wave expansion remains a question in itself and needs further investigation.

Scientists are working towards developing more precise tools for measuring ever short time intervals, aiming to understand and control the behavior of molecules with unprecedented accuracy. A notable example is the true attopump-attoprobe setup. It has been a major challenge due to the difficulty in achieving high photon flux for attosecond pulses. This difficulty can be solved by, e.g. using free electron lasers, which, however, faces the time jitter problem. Recently, the time jitter problem has been overcome, and the attopump-attoprobe scheme has employed to study electronic responses in liquid water [23].

The combination of ultrafast pump–probe technique and the coincidence detection technique has led to the profound advancements in the field of ultrafast molecular dynamics. This combination of techniques can be extended further, by integrating more related techniques. For example, the timing and control of bimolecular reactions have been made possible by introducing the cold environment, from which the dimer is produced, to the mature combination of the pump–probe and coincidence detection techniques. By bringing in photon number detection, one could possibly perform studies in the crossing field of quantum optics and ultrafast physics. By introducing ultrafast time resolution capability to the field of ultracold atoms, one may time resolve the formation of Bose–Einstein condensation. The list goes on.

In addition, quantum computers are expected to play a pivotal role in simulating and understanding molecular behaviors, closing the gap between theoretical predictions and experimental observations. As we delve into complex reactions in diverse environments, from astrochemsitry to living organisms, the future promises a deeper comprehension and manipulation of molecules as the fundamental building block of matter.

Data availability statement

The data cannot be made publicly available upon publication because they are owned by a third party and the terms of use prevent public distribution. The data that support the findings of this study are available upon reasonable request from the authors.

Acknowledgments

This work was supported by the National Natural Science Foundation of China (Grant Nos. 92150105, 12241407, 11925405, 12274294, and 12304377), the Science and Technology Commission of Shanghai Municipality (Grant Nos. 21ZR1420100 and 23JC1402000), and the Shanghai Pujiang Program (Grant No. 23PJ1402600).

ORCID iDs

Shengzhe Pan https://orcid.org/0000-0003-1758-7576
Wenbin Zhang https://orcid.org/0000-0001-9726-2282
Hongcheng Ni https://orcid.org/0000-0003-4924-0921
Jian Wu https://orcid.org/0000-0002-1318-2291

References

[1] Zewail A H 2000 Femtochemistry: atomic-scale dynamics of the chemical bond *J. Phys. Chem.* A **104** 5660

[2] Ferray M, L'Huillier A, LI X F, Lompré L A, Mainfray G and Manus C 1988 Multipleharmonic conversion of 1064-nm radiation in rare-gases *J. Phys. B: At. Mol. Opt. Phys.* **21** L31

[3] Huillier A L, Schafer K J and Kulander K C 1991 Theoretical aspects of intense field harmonic generation *J. Phys. B: At. Mol. Opt. Phys.* **24** 3315

[4] Krause J L, Schafer K J and Kulander K C 1992 High-order harmonic generation from atoms and ions in the high intensity regime *Phys. Rev. Lett.* **68** 3535

[5] Corkum P B 1993 Plasma perspective on strong field multiphoton ionization *Phys. Rev. Lett.* **71** 1994

[6] Schafer K J, Yang B, DiMauro L F and Kulander K C 1993 Above threshold ionization beyond the high harmonic cutoff *Phys. Rev. Lett.* **70** 1599

[7] Macklin J J, Kmetec J D and Gordon C L 1993 High-order harmonic generation using intense femtosecond pulses *Phys. Rev. Lett.* **70** 766

[8] Lewenstein M, Balcou P, Ivanov M Y, L'Huillier A and Corkum P B 1994 Theory of high-harmonic generation by low-frequency laser fields *Phys. Rev.* A **49** 2117

[9] Popmintchev T, Chen M-C, Arpin P, Murnane M M and Kapteyn H C 2010 The attosecond nonlinear optics of bright coherent x-ray generation *Nat. Photon.* **4** 822

[10] Paul P M, Toma E S, Breger P, Mullot G, Augé F, Balcou P, Muller H G and Agostini P 2001 Observation of a train of attosecond pulses from high harmonic generation *Science* **292** 1689

[11] Hentschel M, Kienberger R, Spielmann C, Reider G A, Milosevic N, Brabec T, Corkum P, Heinzmann U, Drescher M and Krausz F 2001 Attosecond metrology *Nature* **414** 509

[12] Uiberacker M *et al* 2007 Attosecond real-time observation of electron tunnelling in atoms *Nature* **446** 627

[13] Lépine F, Ivanov M Y and Vrakking M J J 2014 Attosecond molecular dynamics: fact or fiction? *Nat. Photon.* **8** 195

[14] Jordan I, Huppert M, Rattenbacher D, Peper M, Jelovina D, Perry C, von Conta A, Schild A and Wörner H J 2020 Attosecond spectroscopy of liquid water *Science* **369** 974

[15] Gong X, Heck S, Jelovina D, Perry C, Zinchenko K, Lucchese R and Wörner H J 2022 Attosecond spectroscopy of size-resolved water clusters *Nature* **609** 507

[16] Schultze M *et al* 2013 Controlling dielectrics with the electric field of light *Nature* **493** 75

[17] Tao Z, Chen C, Szilvási T, Keller M, Mavrikakis M, Kapteyn H and Murnane M 2016 Direct time-domain observation of attosecond final-state lifetimes in photoemission from solids *Science* **353** 62

[18] Ciappina M F *et al* 2017 Attosecond physics at the nanoscale *Rep. Prog. Phys.* **80** 054401

[19] Krausz F and Ivanov M 2009 Attosecond physics *Rev. Mod. Phys.* **81** 163

[20] Ma Y, Ni H and Wu J 2023 Attosecond ionization time delays in strong-field physics *Chin. Phys.* B **33** 13201

[21] Fabris D, Witting T, Okell W A, Walke D J, Matia-Hernando P, Henkel J, Barillot T R, Lein M, Marangos J P and Tisch J W G 2015 Synchronized pulses generated at 20 eV and 90 eV for attosecond pump–probe experiments *Nat. Photon.* **9** 383

[22] Kretschmar M, Svirplys E, Volkov M, Witting T, Nagy T, Vrakking M J J and Schütte B 2024 Compact realization of all-attosecond pump-probe spectroscopy *Sci. Adv.* **10** eadk9605

[23] Li S *et al* 2024 Attosecond-pump attosecond-probe x-ray spectroscopy of liquid water *Science* **383** 1118

[24] Itatani J, Quéré F, Yudin G L, Ivanov M Y, Krausz F and Corkum P B 2002 Attosecond streak camera *Phys. Rev. Lett.* **88** 173903

[25] Mairesse Y *et al* 2003 Attosecond synchronization of high-harmonic soft x-rays *Science* **302** 1540

[26] Eckle P, Pfeiffer A N, Cirelli C, Staudte A, Dörner R, Muller H G, Büttiker M and Keller U 2008 Attosecond ionization and tunneling delay time measurements in helium *Science* **322** 1525

[27] Eckle P, Smolarski M, Schlup P, Biegert J, Staudte A, Schöffler M, Muller H G, Dörner R and Keller U 2008 Attosecond angular streaking *Nat. Phys.* **4** 565

[28] Wu J, Meckel M, Schmidt L P H, Kunitski M, Voss S, Sann H, Kim H, Jahnke T, Czasch A and Dörner R 2012 Probing the tunnelling site of electrons in strong field enhanced ionization of molecules *Nat. Commun.* **3** 1113

[29] Dörner R, Mergel V, Jagutzki O, Spielberger L, Ullrich J, Moshammer R and Schmidt-Böcking H 2000 Cold target recoil ion momentum spectroscopy: a 'momentum microscope' to view atomic collision dynamics *Phys. Rep.* **330** 95

[30] Li H, Gong X, Ni H, Lu P, Luo X, Wen J, Yang Y, Qian X, Sun Z and Wu J 2022 Light-induced ultrafast molecular dynamics: from photochemistry to optochemistry *J. Phys. Chem. Lett.* **13** 5881

[31] Roy K *et al* 2024 Optochemical control of slow-wave sleep in the nucleus accumbens of male mice by a photoactivatable allosteric modulator of adenosine A_{2A} receptors *Nat. Commun.* **15** 3661

[32] Klünder K *et al* 2011 Probing single-photon ionization on the attosecond time scale *Phys. Rev. Lett.* **106** 143002

[33] Huppert M, Jordan I, Baykusheva D, von Conta A and Wörner H J 2016 Attosecond delays in molecular photoionization *Phys. Rev. Lett.* **117** 093001

[34] Nandi S *et al* 2020 Attosecond timing of electron emission from a molecular shape resonance *Sci. Adv.* **6** eaba7762

[35] Gruson V *et al* 2016 Attosecond dynamics through a Fano resonance: monitoring the birth of a photoelectron *Science* **354** 734

[36] Kaldun A *et al* 2016 Observing the ultrafast buildup of a Fano resonance in the time domain *Science* **354** 738

[37] Wigner E P 1955 Lower limit for the energy derivative of the scattering phase shift *Phys. Rev.* **98** 145

[38] Smith F T 1960 Lifetime matrix in collision theory *Phys. Rev.* **118** 349

[39] Dahlström J M, L'Huillier A and Maquet A 2012 Introduction to attosecond delays in photoionization *J. Phys. B: At. Mol. Opt. Phys.* **45** 183001

[40] Dahlström J M, Guénot D, Klünder K, Gisselbrecht M, Mauritsson J, L'Huillier A, Maquet A and Taïeb R 2013 Theory of attosecond delays in laser-assisted photoionization *Chem. Phys.* **414** 53

[41] Jiang W *et al* 2022 Atomic partial wave meter by attosecond coincidence metrology *Nat. Commun.* **13** 5072

[42] Kruit P and Read F H 1983 Magnetic field paralleliser for 2π electron-spectrometer and electron-image magnifier *J. Phys.* E **16** 313

[43] Palatchi C, Dahlström J M, Kheifets A S, Ivanov I A, Canaday D M, Agostini P and DiMauro L F 2014 Atomic delay in helium, neon, argon and krypton *J. Phys. B: At. Mol. Opt. Phys.* **47** 245003

[44] Wang A L, Serov V V, Kamalov A, Bucksbaum P H, Kheifets A and Cryan J P 2021 Role of nuclear-electronic coupling in attosecond photoionization of H_2 *Phys. Rev.* A **104** 063119

[45] Jordan I, Huppert M, Pabst S, Kheifets A S, Baykusheva D and Wörner H J 2017 Spin-orbit delays in photoemission *Phys. Rev.* A **95** 013404

[46] Alexandridi C *et al* 2021 Attosecond photoionization dynamics in the vicinity of the Cooper minima in argon *Phys. Rev. Res.* **3** L012012

[47] Swoboda M, Fordell T, Klünder K, Dahlström J M, Miranda M, Buth C, Schafer K J, Mauritsson J, L'Huillier A and Gisselbrecht M 2010 Phase measurement of resonant two-photon ionization in helium *Phys. Rev. Lett.* **104** 103003

[48] Eppink A T J B and Parker D H 1997 Velocity map imaging of ions and electrons using electrostatic lenses: application in photoelectron and photofragment ion imaging of molecular oxygen *Rev. Sci. Instrum.* **68** 3477

[49] Liang J, Han M, Liao Y, Ji J-B, Leung C S, Jiang W-C, Ueda K, Zhou Y, Lu P and Wörner H J 2024 Attosecond-resolved non-dipole photoionization dynamics *Nat. Photon.* **18** 311

[50] Loriot V *et al* 2024 Attosecond metrology of the two-dimensional charge distribution in molecules *Nat. Phys.* **20** 765–9

[51] Heck S, Han M, Jelovina D, Ji J-B, Perry C, Gong X, Lucchese R, Ueda K and Wörner H J 2022 Two-center interference in the photoionization delays of Kr_2 *Phys. Rev. Lett.* **129** 133002

[52] Cattaneo L, Vos J, Bello R Y, Palacios A, Heuser S, Pedrelli L, Lucchini M, Cirelli C, Martín F and Keller U 2018 Attosecond coupled electron and nuclear dynamics in dissociative ionization of H_2 *Nat. Phys.* **14** 733

[53] Isinger M *et al* 2017 Photoionization in the time and frequency domain *Science* **358** 893

[54] Gong X, Plésiat É, Palacios A, Heck S, Martín F and Wörner H J 2023 Attosecond delays between dissociative and non-dissociative ionization of polyatomic molecules *Nat. Commun.* **14** 4402

[55] Vos J, Cattaneo L, Patchkovskii S, Zimmermann T, Cirelli C, Lucchini M, Kheifets A, Landsman A S and Keller U 2018 Orientation-dependent stereo Wigner time delay and electron localization in a small molecule *Science* **360** 1326

[56] Heck S, Baykusheva D, Han M, Ji J-B, Perry C, Gong X and Wörner H J 2021 Attosecond interferometry of shape resonances in the recoil frame of CF_4 *Sci. Adv.* **7** eabj8121

[57] Gong X, Jiang W, Tong J, Qiang J, Lu P, Ni H, Lucchese R, Ueda K and Wu J 2022 Asymmetric attosecond photoionization in molecular shape resonance *Phys. Rev.* X **12** 011002

[58] Ahmadi H *et al* 2022 Attosecond photoionisation time delays reveal the anisotropy of the molecular potential in the recoil frame *Nat. Commun.* **13** 1242

[59] Reid K L 2003 Photoelectron angular distributions *Annu. Rev. Phys. Chem.* **54** 397

[60] Heuser S *et al* 2016 Angular dependence of photoemission time delay in helium *Phys. Rev.* A **94** 063409

[61] Cirelli C *et al* 2018 Anisotropic photoemission time delays close to a Fano resonance *Nat. Commun.* **9** 955

[62] Busto D *et al* 2019 Fano's propensity rule in angle-resolved attosecond pump-probe photoionization *Phys. Rev. Lett.* **123** 133201

[63] Fuchs J, Douguet N, Donsa S, Martin F, Burgdörfer J, Argenti L, Cattaneo L and Keller U 2020 Time delays from one-photon transitions in the continuum *Optica* **7** 154

[64] Joseph J, Holzmeier F, Bresteau D, Spezzani C, Ruchon T, Hergott J F, Tcherbakoff O, D'Oliveira P, Houver J C and Dowek D 2020 Angle-resolved studies of XUV–IR two-photon ionization in the RABBITT scheme *J. Phys. B: At. Mol. Opt. Phys* **53** 184007

[65] Peschel J *et al* 2022 Attosecond dynamics of multi-channel single photon ionization *Nat. Commun.* **13** 5205

[66] Boyer A, Loriot V, Nandi S and Lépine F 2024 Probing photoionization dynamics in acetylene with angle-resolved attosecond interferometry *J. Phys. Chem.* A **128** 840

[67] Autuori A *et al* 2022 Anisotropic dynamics of two-photon ionization: an attosecond movie of photoemission *Sci. Adv.* **8** eabl7594

[68] Clarke D D A, Armstrong G S J, Brown A C and van der Hart H W 2018 R-matrix-with-time-dependence theory for ultrafast atomic processes in arbitrary light fields *Phys. Rev.* A **98** 053442

[69] Moore L R, Lysaght M A, Nikolopoulos L A A, Parker J S, van der Hart H W and Taylor K T 2011 The RMT method for many-electron atomic systems in intense short-pulse laser light *J. Mod. Opt.* **58** 1132

[70] Brown A C, Armstrong G S J, Benda J, Clarke D D A, Wragg J, Hamilton K R, Mašín Z, Gorfinkiel J D and van der Hart H W 2020 RMT: r-matrix with time-dependence. Solving the semi-relativistic, time-dependent Schrödinger equation for general, multielectron atoms and molecules in intense, ultrashort, arbitrarily polarized laser pulses *Comput. Phys. Commun.* **250** 107062

[71] Maquet A and Taïeb R 2007 Two-colour IR+XUV spectroscopies: the "soft-photon approximation" *J. Mod. Opt.* **54** 1847

[72] Jiang W *et al* 2023 Resolving quantum interference black box through attosecond photoionization spectroscopy *Phys. Rev. Lett.* **131** 203201

[73] Han M, Ji J-B, Balčiūnas T, Ueda K and Wörner H J 2023 Attosecond circular-dichroism chronoscopy of electron vortices *Nat. Phys.* **19** 230

[74] Han M, Ji J-B, Leung C S, Ueda K and Wörner H J 2024 Separation of photoionization and measurement-induced delays *Sci. Adv.* **10** eadj2629

[75] Bharti D, Srinivas H, Shobeiry F, Hamilton K R, Moshammer R, Pfeifer T, Bartschat K and Harth A 2023 Multisideband interference structures observed via high-order photon-induced continuum-continuum transitions in argon *Phys. Rev.* A **107** 022801

[76] Bharti D, Srinivas H, Shobeiry F, Bondy A T, Saha S, Hamilton K R, Moshammer R, Pfeifer T, Bartschat K and Harth A 2024 Multi-sideband interference structures by high-order photon-induced continuum-continuum transitions in helium *Phys. Rev.* A **109** 023110

[77] Su J, Ni H, Jaroń-Becker A and Becker A 2014 Time delays in two-photon ionization *Phys. Rev. Lett.* **113** 263002

[78] Freeman R R, Bucksbaum P H, Milchberg H, Darack S, Schumacher D and Geusic M E 1987 Above-threshold ionization with subpicosecond laser pulses *Phys. Rev. Lett.* **59** 1092

[79] Gong X *et al* 2017 Energy-resolved ultrashort delays of photoelectron emission clocked by orthogonal two-color laser fields *Phys. Rev. Lett.* **118** 143203

[80] Kitzler M and Lezius M 2005 Spatial control of recollision wave packets with attosecond precision *Phys. Rev. Lett.* **95** 253001

[81] Brugnera L, Hoffmann D J, Siegel T, Frank F, Zaïr A, Tisch J W G and Marangos J P 2011 Trajectory selection in high harmonic generation by controlling the phase between orthogonal two-color fields *Phys. Rev. Lett.* **107** 153902

[82] Xie X 2015 Two-dimensional attosecond electron wave-packet interferometry *Phys. Rev. Lett.* **114** 173003

[83] Tong J *et al* 2022 Probing resonant photoionization time delay by self-referenced molecular attoclock *Phys. Rev. Lett.* **129** 173201

[84] Kleimenov E, Piticco L and Merkt F 2008 Spectroscopic characterization and potential energy functions of the six low-lying electronic states of ArKr+ *Mol. Phys.* **106** 1835

[85] Gokhberg K, Kolorenč P, Kuleff A I and Cederbaum L S 2014 Site- and energy-selective slow-electron production through intermolecular Coulombic decay *Nature* **505** 661

[86] Feynman R P 1948 Space-time approach to non-relativistic quantum mechanics *Rev. Mod. Phys.* **20** 367

[87] Yan T-M, Popruzhenko S V, Vrakking M J J and Bauer D 2010 Low-energy structures in strong field ionization revealed by quantum orbits *Phys. Rev. Lett.* **105** 253002

[88] Song X, Shi G, Zhang G, Xu J, Lin C, Chen J and Yang W 2018 Attosecond time delay of retrapped resonant ionization *Phys. Rev. Lett.* **121** 103201

[89] Ergler T, Rudenko A, Feuerstein B, Zrost K, Schröter C D, Moshammer R and Ullrich J 2006 Spatiotemporal imaging of ultrafast molecular motion: collapse and revival of the D_2^+ nuclear wave packet *Phys. Rev. Lett.* **97** 193001

[90] Kremer M *et al* 2009 Electron localization in molecular fragmentation of H_2 by carrier-envelope phase stabilized laser pulses *Phys. Rev. Lett.* **103** 213003

[91] Xu H, Li Z, He F, Wang X, Atia-Tul-Noor A, Kielpinski D, Sang R T and Litvinyuk I V 2017 Observing electron localization in a dissociating H_2^+ molecule in real time *Nat. Commun.* **8** 15849

[92] Nubbemeyer T, Gorling K, Saenz A, Eichmann U and Sandner W 2008 Strong-field tunneling without ionization *Phys. Rev. Lett.* **101** 233001

[93] Zhang W *et al* 2017 Photon-number-resolved asymmetric dissociative single ionization of H_2 *Phys. Rev.* A **96** 033405

[94] Sainadh U S *et al* 2019 Attosecond angular streaking and tunnelling time in atomic hydrogen *Nature* **568** 75

[95] Klaiber M, Lv Q Z, Sukiasyan S, Bakucz Canário D, Hatsagortsyan K Z and Keitel C H 2022 Reconciling conflicting approaches for the tunneling time delay in strong field ionization *Phys. Rev. Lett.* **129** 203201

[96] Pfeiffer A N, Cirelli C, Smolarski M, Dörner R and Keller U 2011 Timing the release in sequential double ionization *Nat. Phys.* **7** 428

[97] Hanus V, Kangaparambil S, Larimian S, Dorner-Kirchner M, Xie X, Schöffler M S, Paulus G G, Baltuška A, Staudte A and Kitzler-Zeiler M 2019 Subfemtosecond tracing of molecular dynamics during strong-field interaction *Phys. Rev. Lett.* **123** 263201

[98] Hanus V, Kangaparambil S, Larimian S, Dorner-Kirchner M, Xie X, Schöffler M S, Paulus G G, Baltuška A, Staudte A and Kitzler-Zeiler M 2020 Experimental separation of subcycle ionization bursts in strong-field double ionization of H_2 *Phys. Rev. Lett.* **124** 103201

[99] Wu J *et al* 2013 Understanding the role of phase in chemical bond breaking with coincidence angular streaking *Nat. Commun.* **4** 2177

[100] Mi Y *et al* 2020 Clocking enhanced ionization of hydrogen molecules with rotational wave packets *Phys. Rev. Lett.* **125** 173201

[101] Kling M F *et al* 2006 Control of electron localization in molecular dissociation *Science* **312** 246

[102] Sansone G *et al* 2010 Electron localization following attosecond molecular photoionization *Nature* **465** 763

[103] Fischer B, Kremer M, Pfeifer T, Feuerstein B, Sharma V, Thumm U, Schröter C D, Moshammer R and Ullrich J 2010 Steering the electron in H_2 by nuclear wave packet dynamics *Phys. Rev. Lett.* **105** 223001

[104] Rathje T, Sayler A M, Zeng S, Wustelt P, Figger H, Esry B D and Paulus G G 2013 Coherent control at its most fundamental: carrier-envelope-phase-dependent electron localization in photodissociation of a H_2^+ molecular ion beam target *Phys. Rev. Lett.* **111** 093002

[105] Gong X, He P, Song Q, Ji Q, Pan H, Ding J, He F, Zeng H and Wu J 2014 Two-dimensional directional proton emission in dissociative ionization of H_2 *Phys. Rev. Lett.* **113** 203001

[106] Ray D *et al* 2009 Ion-energy dependence of asymmetric dissociation of D_2 by a two-color laser field *Phys. Rev. Lett.* **103** 223201

[107] Wu J, Vredenborg A, Schmidt L P H, Jahnke T, Czasch A and Dörner R 2013 Comparison of dissociative ionization of H_2, N_2, Ar_2, and CO by elliptically polarized two-color pulses *Phys. Rev.* A **87** 023406

[108] Ji Q *et al* 2019 Timing dissociative ionization of H_2 using a polarization-skewed femtosecond laser pulse *Phys. Rev. Lett.* **123** 233202

[109] Karras G, Ndong M, Hertz E, Sugny D, Billard F, Lavorel B and Faucher O 2015 Polarization shaping for unidirectional rotational motion of molecules *Phys. Rev. Lett.* **114** 103001

[110] Tutunnikov I, Gershnabel E, Gold S and Averbukh I S 2018 Selective orientation of chiral molecules by laser fields with twisted polarization *J. Phys. Chem. Lett.* **9** 1105

[111] Kang L, Ilia T, Junyang M, Junjie Q, Lianrong Z, Olivier F, Yehiam P, Ilya Sh A and Jian W 2020 Spatiotemporal rotational dynamics of laser-driven molecules *Adv. Photon.* **2** 024002

[112] Xu L, Tutunnikov I, Zhou L, Lin K, Qiang J, Lu P, Prior Y, Averbukh I S and Wu J 2020 Echoes in unidirectionally rotating molecules *Phys. Rev.* A **102** 043116

[113] Neyra E G, Videla F, Biasetti D A, Ciappina M F and Rebón L 2023 Twisting attosecond pulse trains by amplitude-polarization IR pulses *Phys. Rev.* A **108** 043102

[114] Pan S *et al* 2021 Clocking dissociative above-threshold double ionization of H_2 in a multicycle laser pulse *Phys. Rev. Lett.* **126** 063201

[115] Seideman T, Ivanov M Y and Corkum P B 1995 Role of electron localization in intense-field molecular ionization *Phys. Rev. Lett.* **75** 2819

[116] Zuo T and Bandrauk A D 1995 Charge-resonance-enhanced ionization of diatomic molecular ions by intense lasers *Phys. Rev.* A **52** R2511

[117] Esry B D, Sayler A M, Wang P Q, Carnes K D and Ben-Itzhak I 2006 Above threshold coulomb explosion of molecules in intense laser pulses *Phys. Rev. Lett.* **97** 013003

[118] Madsen C B, Anis F, Madsen L B and Esry B D 2012 Multiphoton above threshold effects in strong-field fragmentation *Phys. Rev. Lett.* **109** 163003

[119] Pan S *et al* 2022 Low-energy protons in strong-field dissociation of H_2^+ via dipole-transitions at large bond lengths ultrafast *Science* **2022** 9863548

[120] Pan S *et al* 2023 Manipulating parallel and perpendicular multiphoton transitions in H_2 molecules *Phys. Rev. Lett.* **130** 143203

[121] Luo Z, Chang Y, Zhao Y, Yang J, Chen Z, Cheng Y, Che L, Wu G, Yang X and Yuan K 2021 Photodissociation dynamics of H_2O via the $\tilde{E}'(^1B_2)$ electronic state *J. Phys. Chem.* A **125** 3622

[122] Chang Y *et al* 2020 Electronically excited OH super-rotors from water photodissociation by using vacuum ultraviolet free-electron laser pulses *J. Phys. Chem. Lett.* **11** 7617

[123] Chang Y *et al* 2019 Hydroxyl super rotors from vacuum ultraviolet photodissociation of water *Nat. Commun.* **10** 1250

[124] Lin K *et al* 2020 Femtosecond resolving photodissociation dynamics of the SO_2 molecule *J. Phys. Chem. Lett.* **11** 3129

[125] Iglesias H A and Chirife J 1976 Prediction of the effect of temperature on water sorption isotherms of food material *Int. J. Food Sci. Technol.* **11** 109

[126] Pollard J E, Lichtin D A and Cohen R B 1988 Differential cross sections for state-selected reactions in the $H_2^+ + H_2$ system *Chem. Phys. Lett.* **152** 171

[127] Zhang Y *et al* 2020 Formation of H_3^+ from ethane dication induced by electron impact *Commun. Chem.* **3** 160

[128] De S, Rajput J, Roy A, Ghosh P N and Safvan C P 2006 Formation of H_3^+ due to intramolecular bond rearrangement in doubly charged methanol *Phys. Rev. Lett.* **97** 213201

[129] Jochim B, Lueking A, Doshier L, Carey S, Wells E, Parke E, Leonard M, Carnes K D and Ben-Itzhak I 2009 Rapid formation of H_3^+ from ammonia and methane following 4 MeV proton impact *J. Phys. B: At. Mol. Opt. Phys.* **42** 091002

[130] Oka T 1980 Observation of the infrared spectrum of H_3^+ *Phys. Rev. Lett.* **45** 531

[131] Buelow S, Radhakrishnan G, Catanzarite J and Wittig C 1985 The use of van der Waals forces to orient chemical reactants: the H+CO_2 reaction *J. Chem. Phys.* **83** 444

[132] Scherer N F, Khundkar L R, Bernstein R B and Zewail A H 1987 Real-time picosecond clocking of the collision complex in a bimolecular reaction: the birth of OH from H+CO_2 *J. Chem. Phys.* **87** 1451

[133] Zhou L *et al* 2023 Ultrafast formation dynamics of D_3^+ from the light-driven bimolecular reaction of the D_2–D_2 dimer *Nat. Chem.* **15** 1229

[134] Mi Y, Wang E, Dube Z, Wang T, Naumov A Y, Villeneuve D M, Corkum P B and Staudte A 2023 $D_3{}^+$ formation through photoionization of the molecular D_2–D_2 dimer *Nat. Chem.* **15** 1224

[135] Hogness T R and Lunn E G 1925 The ionization of hydrogen by electron impact as interpreted by positive ray analysis *Phys. Rev.* **26** 44

[136] McCall B J and Oka T 2000 $H_3{}^+$–an ion with many talents *Science* **287** 1941

[137] McGuire B A, Asvany O, Brünken S and Schlemmer S 2020 Laboratory spectroscopy techniques to enable observations of interstellar ion chemistry *Nat. Rev. Phys.* **2** 402

[138] Eland J H D 1996 The origin of primary H_3^+ ions in mass spectra *Rapid Commun. Mass Spectrom.* **10** 1560

[139] Wang E, Ren X and Dorn A 2021 Role of the environment in quenching the production of H_3^+ from dicationic clusters of methanol *Phys. Rev. Lett.* **126** 103402

[140] Furukawa Y, Hoshina K, Yamanouchi K and Nakano H 2005 Ejection of triatomic hydrogen molecular ion from methanol in intense laser fields *Chem. Phys. Lett.* **414** 117

[141] Livshits E, Luzon I, Gope K, Baer R and Strasser D 2020 Time-resolving the ultrafast H_2 roaming chemistry and H_3^+ formation using extreme-ultraviolet pulses *Commun. Chem.* **3** 49

[142] Okino T, Furukawa Y, Liu P, Ichikawa T, Itakura R, Hoshina K, Yamanouchi K and Nakano H 2006 Coincidence momentum imaging of ultrafast hydrogen migration in methanol and its isotopomers in intense laser fields *Chem. Phys. Lett.* **423** 220

[143] Hoshina K, Furukawa Y, Okino T and Yamanouchi K 2008 Efficient ejection of H_3^+ from hydrocarbon molecules induced by ultrashort intense laser fields *J. Chem. Phys.* **129** 104302

[144] Kraus P M, Schwarzer M C, Schirmel N, Urbasch G, Frenking G and Weitzel K-M 2011 Unusual mechanism for H_3^+ formation from ethane as obtained by femtosecond laser pulse ionization and quantum chemical calculations *J. Chem. Phys.* **134** 114302

[145] Kotsina N, Kaziannis S and Kosmidis C 2014 Hydrogen migration in methanol studied under asymmetric fs laser irradiation *Chem. Phys. Lett.* **604** 27

[146] Ekanayake N, Nairat M, Weingartz N P, Michie M J, Levine B G and Dantus M 2018 Substituent effects on H_3^+ formation via H_2 roaming mechanisms from organic molecules under strong-field photodissociation *J. Chem. Phys.* **149** 244310

[147] Ekanayake N *et al* 2017 Mechanisms and time-resolved dynamics for trihydrogen cation (H_3^+) formation from organic molecules in strong laser fields *Sci. Rep.* **7** 4703

[148] Ekanayake N *et al* 2018 H_2 roaming chemistry and the formation of H_3^+ from organic molecules in strong laser fields *Nat. Commun.* **9** 5186

[149] Zhou L *et al* 2023 Stereodynamical control of D_3^+ formation from the bimolecular photoreaction in the D_2–D_2 dimer *J. Phys. Chem. Lett.* **14** 10348

[150] Wang Y, Huang J, Wang W, Du T, Xie Y, Ma Y, Xiao C, Zhang Z, Zhang D H and Yang X 2023 Stereodynamical control of the $H + HD \rightarrow H_2 + D$ reaction through HD reagent alignment *Science* **379** 191

[151] Buelow S, Noble M, Radhakrishnan G, Reisler H, Wittig C and Hancock G 1986 The role of initial conditions in elementary gas-phase processes involving intermediate "complexes" *J. Phys. Chem.* **90** 1015

[152] Shi M, Huang H, Lu C, Zhou L, Jiang Z, Ni H, Zhang W and Wu J 2024 Impact of nuclear motion on light-induced bimolecular interaction dynamics *Phys. Rev.* X **14** 041001

[153] Jiang Z *et al* 2024 Ultrafast photoinduced C-H bond formation from two small inorganic molecules *Nat. Commun.* **15** 2854

[154] Huang H, Hou H, Wen J, Ni H and Wu J 2024 Ultrafast formation dynamics of D_3^+ from bimolecular reaction of the D_2-D_2 dimer *Phys. Rev.* A **109** 043107

[155] Feuerstein B and Thumm U 2003 On the computation of momentum distributions within wavepacket propagation calculations *J. Phys. B: At. Mol. Opt. Phys.* **36** 707

[156] Wang X, Tian J and Eberly J H 2013 Extended virtual detector theory for strong-field atomic ionization *Phys. Rev. Lett.* **110** 243001

[157] Wang X, Tian J and Eberly J H 2018 Virtual detector theory for strong-field atomic ionization *J. Phys. B: At. Mol. Opt. Phys.* **51** 084002

[158] Xu R-H and Wang X 2021 Extended virtual detector theory including quantum interferences *AIP Adv.* **11** 025124

[159] Lai X Y, Cai Q-Y and Zhan M S 2009 From a quantum to a classical description of intense laser–atom physics with Bohmian trajectories *New J. Phys.* **11** 113035

[160] Lai X-Y and Liu X-J 2020 Bohmian trajectory perspective on strong field atomic processes *Chin. Phys.* B **29** 013205

[161] Ni H, Saalmann U and Rost J-M 2018 Tunneling exit characteristics from classical backpropagation of an ionized electron wave packet *Phys. Rev.* A **97** 013426

[162] Ni H, Eicke N, Ruiz C, Cai J, Oppermann F, Shvetsov-Shilovski N I and Pi L-W 2018 Tunneling criteria and a nonadiabatic term for strong-field ionization *Phys. Rev.* A **98** 013411

[163] Ni H, Saalmann U and Rost J-M 2016 Tunneling ionization time resolved by backpropagation *Phys. Rev. Lett.* **117** 023002